Plant Physiology Preview. Published on June 26, 2017, as DOI:10.1104/pp.17.00433

Identification and metabolite profiling of chemical activators of lipid accumulation in green algae

Nishikant Wase, Boqiang Tu, James W. Allen, Paul Black and Concetta DiRusso*

Department of Biochemistry, University of Nebraska, Lincoln, NE 68588, *USA*

*Address correspondence: to *cdirusso2@unl.edu*

Author Contributions

C.D. and N.W. conceived the original compound selection and screening plan. N.W., J.W.A. and B.T. performed the research. C.D., N.W., J.W.A. and B.T. analyzed the data and C.D., N.W., J.W.A. and P.N.B. wrote the article and prepared the figures and tables**.**

Short Title:

Metabolite profiles of algal lipid activators

One sentence summary:

Small compound activators of lipid accumulation in algae are distinguished by differential effects on lipid and polar metabolite profiles.

ABSRACT

Microalgae are proposed as feedstock organisms useful for producing biofuels and co-products. However, several limitations must be overcome before algae-based production is economically feasible. Among these is the ability to induce lipid accumulation and storage without affecting biomass yield. To overcome this barrier, a chemical genetics approach was employed in which 43,783 compounds were screened against *Chlamydomonas reinhardtii* and 243 compounds were identified that increase triacylglyceride (TAG) accumulation without terminating growth. Identified compounds were classified by structural similarity and 15 were selected for secondary analyses addressing impacts on growth fitness, photosynthetic pigments, and total cellular protein and starch concentrations. TAG accumulation was verified using GC-MS quantification of total fatty acids and targeted TAG and galactolipid (GL) measurements using LC-MRM/MS. These results demonstrated TAG accumulation does not necessarily proceed at the expense of GL. Untargeted metabolite profiling provided important insights into pathway shifts due to 5 different compound treatments and verified the anabolic state of the cells with regard to the oxidative pentose phosphate pathway, Calvin cycle, tricarboxylic acid cycle and amino acid biosynthetic pathways. Metabolite patterns were distinct from nitrogen starvation and other abiotic stresses commonly used to induce oil accumulation in algae. The efficacy of these compounds was also demonstrated in 3 other algal species. These lipid inducing compounds offer a valuable set of tools for delving into the biochemical mechanisms of lipid accumulation in algae and a direct means to improve algal oil content independent of the severe growth limitations associated with nutrient deprivation.

Keywords: algae, biofuels, bioproducts, high throughput screening, lipids, metabolite profiles

INTRODUCTION

Currently economic barriers must be overcome for the commercial adoption of microalgae for next generation biofuel production despite their distinct advantages. These include rapid growth and the ability to accumulate 20-40% of dry weight as lipids, a potential for 100-fold more oil per acre than soybeans or other oil-seed bearing plants, and an ability to thrive in poor quality water in a large variety of environmental conditions (Jones and Mayfield, 2012; Scranton et al., 2015). Algae also fix CO_2 into biomass during photosynthesis, thus addressing concerns about the generation of carbon emissions. Additionally, a wide range of byproducts useful for biotechnological applications are produced in algae, notably replacing an increasing amount of the docosahexaenoic acid (DHA, C22:6 ω3) market as the supply of fish oil dwindles (Morita et al., 2006; Song et al., 2015).

Lipid accumulation in algae normally requires an environmental stress, particularly nutrient deprivation of nitrogen, sulfur or certain metals, as algae do not appreciably synthesize oil during rapid growth (Guarnieri et al., 2011; Cakmak et al., 2012). Nutrient limitation is sometimes achieved during normal growth when cultures reach saturation density when nitrogen becomes limiting and triacylglyceride (TAG) rich lipid droplets become visible and measurable (Msanne et al., 2012; Wang et al., 2012). This is normally preceded by, or commensurate with, cessation of protein synthesis, degradation of chlorophylls and photosynthetic enzymes including RuBisCO, and a dramatic reduction in chloroplast membrane lipids (Wase et al., 2014; Allen et al., 2015). Therefore, the commercial production of algae for fuel and coproducts is limited by the antagonism between reproductive growth and oil accumulation. Solving this problem requires further insight into activating metabolic pathways leading to lipid storage while avoiding the obstruction of cell growth or division.

Important information on lipid synthetic pathways has been derived by comparison of algal and plant genomes (Awai et al., 2006; Benning, 2008). Such comparisons have led to the conclusion that fatty acid synthesis in algae occurs primarily, if not exclusively, in the chloroplast (reviewed in (Hu et al., 2008)). Fatty acid synthesis uses metabolic substrates derived from photosynthetic CO_2 fixation, which supplies chloroplast-specific complex lipid synthesis. *De novo* synthesized fatty acids must also be trafficked outside the chloroplast to support extra-plastid lipid synthesis (Awai et al., 2006). Involved in this process is an interwoven, intracellular

system of acyl chain incorporation into glycerolipids including the Kennedy Pathway, acyl chain editing and lipid remodeling reactions. During N starvation, this system is coopted for TAG synthesis, which competes with membrane lipid synthesis for available acyl-CoA. In algae, abiotic stress-induced TAG synthesis mainly occurs through the sequential acylation of glycerol using fatty acids derived from both *de novo* synthesis and membrane glycerolipids, which are continually synthesized and degraded (Allen et al., 2015). The side chain composition of newly synthesized TAG, however, differs significantly from membrane lipid fatty acid composition in having higher levels of saturated and monounsaturated long chain fatty acids, supporting a greater role for *de novo* synthesized acyl chain incorporation (reviewed in (Hu et al., 2008)). Additionally, ^{13}C-CO_2 labeling provides evidence that a large majority of the TAG side chains are derived directly from photosynthetic CO_2 fixation and *de novo* fatty acid synthesis (Allen et al., 2015; Allen et al., 2017). These recent advancements indicate that, although membrane glycerolipid synthesis, degradation, and acyl editing are intricately involved in TAG accumulation as a consequence of the stress-induced cessation of growth, it may be possible to extricate TAG synthesis from these reactions.

In previous studies, we used a combinatorial proteomics and metabolomics approach to help define metabolic and regulatory mechanisms responsible for TAG synthesis, especially related to the central metabolism during nitrogen starvation (Wase et al., 2014). These studies indicated that the TCA cycle acts as a central hub for maintaining equilibrium in the supply and demand of carbon skeletons, channeling excess carbon precursors as citrate into lipid synthesis (Wase et al., 2014). Under these conditions growth is halted, biosynthetic activities are minimized, and excess carbon is channeled to lipids. Thus, the yield of biomass is compromised, which ultimately also limits lipid production and thus minimizes feasibility for use in biofuels.

Here we report a chemical genetics study using small molecule activators of lipid synthesis that were identified by high throughput screening. Several of these lipid activators were employed to probe pathways permissive to both algal growth and TAG accumulation (McCourt and Desveaux, 2010; Wase et al., 2015). For screening, low density algal cultures were treated with compounds from a large chemical library for 72 h, and both growth and lipid accumulation were assessed (Wase et al., 2015). A collection of 243 active compounds were identified and verified that fell into 5 structurally-related groups. Novel secondary screens were conducted with 15 of these compounds to examine impacts on growth and chloroplast integrity,

as well as total lipid, protein, and starch contents. All but one compound accumulated TAG without producing an apparent stress response. To further these analyses, metabolite profiles resulting from treatment with a subset of 5 compounds inducing distinct phenotypic responses in *Chlamydomonas reinhardtii* were conducted. These data provide valuable insight into changes in central carbon and amino acid metabolism associated with lipid accumulation in algae. To confirm that TAG accumulation is not limited to *C. reinhardtii*, we also tested the selected compounds in three different freshwater chlorophycean algae: *Chlorella sorokiniana*, *Chlorella vulgaris* and *Tetrachlorella alterens*. Lipid-inducing compounds discovered by chemical genetic screening represent useful tools for identifying metabolic reactions and regulatory factors that can affect both lipid and biomass accumulation, and thus are of use in the commercial production of algal biofuels and other high value co-products.

RESULTS

Selection of lipid storage activators

The screening protocol used was previously devised and tested using a small compound library designed for this purpose (Wase et al., 2015) and is outlined in Supplemental Fig. S1. The primary selection required two phenotypic tests; [1] the lipophilic dye Nile Red was used to identify treated cells that accumulated neutral lipids, and [2] assessment of growth and accumulated cellular mass using spectrophotometric measurements at OD_{600}. Compounds were added to a final concentration of 10 µM at low cell density and cells were cultured for 72 h prior to analyses. In the current screening experiments, a control based normalization approach was employed where the data were standardized to a negative control in terms of lipid accumulation (*i.e.*, cells cultured without compound in Tris-acetate-phosphate media (TAP) with vehicle (DMSO)). For quality control analysis (QC), a Z-factor was calculated for each analysis plate to determine the separation between the positive control for lipid accumulation (cells grown in TAP media without nitrogen (N-)) and the negative control (cells grown in standard TAP media with nitrogen (N+)) to measure the signal range (Zhang et al., 1999). The mean Z-factor was robust at

153 0.78 ± 0.08 over 124 plates that were used to screen 43,783 compounds (Fig.1A). The QC
154 analysis is given in supplemental data 1 (Supplemental Fig. S2-S4).
155 Estimation of the change in biomass after 72h treatment compared with the initial
156 inoculum revealed that 35 of the 43,783 compounds severely blunted growth (*i.e.,* final $OD_{600} \leq$
157 0.2) (Fig. 1B). Approximately 3% of the compounds (1,294) had a moderate inhibitory effect on
158 growth whereby the cells achieved an average optical density ≤ 0.32. Treatment with 26,656
159 compounds resulted in an average of 0.45 OD_{600} after three days of treatment, which was
160 comparable to the controls.
161 Following the elimination of compounds that limited growth, a fold-change analysis of
162 Nile Red intensity as an indicator of neutral lipid accumulation was completed (Fig. 1C). The
163 primary hit list included 367 compounds that induced lipid accumulation to ≥ 2.5-fold levels
164 over untreated controls to yield a hit rate of 0.8%. To confirm the primary screening results,
165 these compounds were retested at over a range of concentrations from 0.25 to 30 μM (Fig. 1D
166 and Supplemental Table S3). Fluorescence microscopy was used to verify these compounds
167 induced lipid body accumulation in cells (data not shown). The final hits from the primary
168 screen consisted of 243 compounds that gave 2.5-fold induction at one or more concentrations
169 tested; 124 compounds that yielded less than 2.5-fold lipid induction were not considered for
170 further analysis (Supplemental Fig. S2, and PubChem AID 1159536).
171
172 **Structural models for lipid-inducing compounds**
173
174 To gain insight into the structural relatedness of the hit compounds, we performed
175 chemoinformatics analysis using cytoscape ChemViz plugin (Wallace et al., 2011). Structural
176 similarity of the compounds were based on Estate bit fingerprint descriptors (Hall and Kier,
177 1995). To construct a network similarity graph, a Tanimoto similarity cutoff of 0.70 was used
178 for edge creation (0 representing dissimilar compounds and 1.0 representing identical
179 compounds) and visualized using Cytoscape v2.8.2 (Yeung et al., 2002). Data from three
180 treatment concentrations, 10, 15 and 30 μM were mapped and a pie chart was painted at each
181 node. The fold change value for data acquired at the 30 μM concentration was used to adjust the
182 node size (Fig. 2).

The analysis using the Cytoscape ChemViz plugin provided a structure-activity relationship in the form of a network similarity graph based on the structural similarities of the compounds and their ability to induce lipid synthesis. For further analysis of the compounds to identify structurally similar molecular framework /scaffolds Scaffold hunter was used (Wetzel et al., 2009). The structures of the 243 active molecules were imported into Scaffold hunter v2.3.0 and a new database was created. Using chemical fingerprinting analysis of the 243 active small molecules, we constructed a model to predict the active structural class of the lipid accumulating compounds. The chemical space was organized by abstracting the molecular structures so that a set of structurally similar molecules can be represented by a single structure referred to as the molecular framework, or scaffold, that is obtained from a molecule by removing side chains, generating a hierarchy of scaffolds sharing a common molecular framework. For structural comparison of the active molecules, first Estate Bit chemical fingerprints were calculated and hierarchical clustering was performed by the Ward's linkage method. The distance was calculated using the Tanimoto coefficient of 0.70 noted above (Hall and Kier, 1995). Based on the hierarchical clustering, we identified several major and minor structural classes of compounds that illustrate related structure and activity. Using at least 3 compounds per cluster, we identified 18 different structural molecular frameworks (scaffolds) and 45 singletons (Fig. 2A and 2B). The major common structural features included benzene (45 members), piperazine (114 members), morpholine (32 members), piperidine (28 members), adamantane (14 members), and cyclopentane (11 members). Further comparisons of the most active compounds in terms of lipid accumulation led to the selection of 15 that were divided into 5 related structural groups. Compounds in group 1 (GR-1) shared a piperidine moiety, group 2 (GR-2) a benzyl piperizine moiety, group 3 (GR-3) a nitrobenzene moiety, group 4 (GR-4) a phenylpiperizine moiety and group 5 (GR-5) an adamantane moiety (Fig. 3).

To visually assess the effect of compounds on the lipid accumulating phenotype, cells were stained with Nile Red and images captured using both brightfield and fluorescent confocal microscopy (Fig. 3). As expected, all compounds induced the accumulation of lipid bodies. For some compound treatments, granular particles were also observed that may be starch deposits.

Effect of selected compounds on growth, photosynthetic pigments, total starch and protein

The 15 highest performing compounds in terms of lipid accumulation and growth were further evaluated using secondary screens that assessed impact on growth and selected cellular metabolite pools. Cells in early-log phase (0.1-0.2 OD_{600}) were treated with compounds at a single concentration of 30 µM. Incubation was continued for 72 h and the change in the optical density was monitored daily (Fig. 4A). At 30 µM, some growth reduction was observed for most compounds after 48 h compared with controls. One compounds WD10784 had a more pronounced reduction of growth at 30 µM, so the concentration of this compounds was reduced to 10 µM for secondary analyses. This concentration was sufficient to induce the maximal lipid accumulation and was less growth restrictive. Importantly, unlike during N starvation, total protein levels were not significantly reduced by treatment with any of the selected lipid activating compounds (Fig. 4B). Protein levels were slightly but significantly increased after treatment with WD10264, WD10872, WD10615, and WD20542.

During N limitation, which induces the accumulation of lipids, the levels of starch also increases, indicating the storage of carbon as both sugars and fats (Longworth et al., 2012). These changes in the macromolecular pools are associated with the stress response induced by N limitation and the redirection of carbon to storage compounds including lipids and starch (Wase et al., 2014). Treatment with the selected lipid inducing compounds had a variable impact on accumulation of starch; 8 compounds had no significant impact on starch accumulation while 7 compounds significantly increased starch levels compared to the untreated control cells (Fig. 5A). The compounds that did not alter starch levels were primarily from structural groups 1 and 3. The most common structural feature of the compounds that induced starch levels was the piperazine moiety, thus suggesting that this structural feature is important in inducing this effect.

To utilize carbon efficiently and satisfy energy demands, algae must maintain adequate chlorophyll and carotenoids levels. We have previously shown that during nitrogen starvation, there is a gradual decrease in the chlorophyll:carotenoid ratio (Wase et al., 2014). Quantification of photosynthetic and total carotenoid pigments showed treatment with most compounds had no significant effect (Fig. 5B-5D). However, treatment for 72h with compounds WD10784 and WD10615 reduced total carotenoids, chlorophyll a (chl a) and chlorophyll b (chl b) by ≥50 %, relative to control levels (Fig. 5B-5D). There was also a small but significant decrease in both carotenoid and chl b quantities after treatment with WD10738, WD10599, and WD20542, while chl a was unaffected.

245

246 **Fatty acid analysis of compound treated cells**

247

248 Following compound treatment of *Chlamydomonas*, lipids were extracted and the fatty
249 acid composition determined using GC-MS (Table 1). The total amount of fatty acids
250 accumulated varied with compound treatment from 1.3-fold (WD40157) to 4.4-fold (WD30030)
251 control cells. For all compound treatments, there were significantly higher levels of C16:0,
252 C18:0, C18:2$^{cis\Delta 9,12}$ and C18:3$^{cis\Delta 9,12,15}$ compared with untreated control cells (given as µg/5x10^6
253 cells). For example, compound WD40844 (Table 1, line 3) resulted in the accumulation of 3.7-
254 fold more C16:0 as compared to untreated control cells; C16:0 was increased 3.8-fold with
255 WD30030 treatment, 3.0-fold with WD20067, 3.2-fold with WD10461, 2.4-fold with WD20542,
256 3.7-fold with WD40844, and 2.6-fold with WD10784. The fatty acid profiles for compound
257 treated cells differed somewhat from those measured after nitrogen starvation (Msanne et al.,
258 2012; Wase et al., 2014). For example, during nitrogen starvation, the levels of the
259 polyunsaturated fatty acid C16:4 increase, whereas for most of the lipid accumulating
260 compounds the levels of this fatty acid were not significantly different from the controls. The
261 opposite was true for C18:3.

262

263 **Complex lipid analysis after selected compound treatments**

264

265 In order to gain further insight into the biochemical shifts that result during treatment of
266 *Chlamydomonas* with compounds from the different structural classes that promoted lipid
267 accumulation, we performed metabolite analyses of cultures treated with WD10784 from GR-1
268 (piperidine moiety), WD10461 from GR-2 (benzyl piperizine moiety), WD30030 from GR-3
269 (nitrobenzene moiety), and WD20067 and WD20542 from GR-5 (adamantane moiety). A
270 common component of the algal abiotic stress response is the reduction of chlorophyll content
271 and concurrent degradation of chloroplast membrane lipids, specifically mono-
272 galactosyldiacylglycerol (MGDG) which can collapse these membranes into irreversible, non-
273 biological states as chloroplasts are dimensionally reduced (Guschina and Harwood, 2009;
274 Goncalves et al., 2013; Urzica et al., 2013). The galactolipid (GL) content of cells was therefore
275 analyzed in relation to TAG levels to assess both the quantitative extent of TAG accumulation

and possible abiotic stress due to the compound treatments (Fig. 6A-6C). In all cases, the compounds increased the TAG content ranging from 2.7 ± 0.6- to 5.5 ± 3.0-fold greater than algae grown without compounds but with vehicle (DMSO) (Fig. 6A). The total GL content of cells treated with WD30030, WD20542, WD10784, and WD10461, was not statistically significant by one-way analysis of variance ($p > 0.05$) (Fig 6B). By contrast, treatment with WD20067 reduced total GL by 0.3 ± 0.04 fold. Therefore, with the exception of WD20067, the compounds tested increased TAG content without causing the chloroplast membrane lipid degradation typical of abiotic stress.

Changes in polar metabolite levels in response to compound treatment

Untargeted metabolomics was employed using GC-MS to broadly assess impacts of the 5 selected compounds on cellular polar metabolites. Identified metabolites were reported if present in at least 7 of 9 samples per treatment group, resulting in a list of 125 compounds. These were deconvoluted and aligned using the eRah R-package. Putative identification of the compounds was made using both the MassBank and Golm metabolome databases, which resulted in 98 unique metabolite identifications. The metabolite IDs were mapped with the KEGG compound IDs and classified according to KEGG compound biological role classifications (Table 2). Metabolites annotated but not assigned a role in the KEGG databases were denoted as unclassified and unannotated metabolites were classified as unknown.

For the first quantitative evaluation, normalized and pareto scaled ion intensities for the 125 metabolites and 54 samples (9 replicates for each condition) were analyzed using unsupervised multivariate statistics (principal component analysis, PCA) to globally compare biochemical traits between the control and compound treated groups. The resultant score scatterplot showed that the principal factors PC1 and PC2 discriminated between the metabolite profiles in accordance with the compound treatment (Fig 7A). PC 1 had an explained variance of 22.2% and mainly discriminated the metabolite profiles of the untreated control from compound treated samples. With the combination of PC2 (explained variance 20.6%), all the treated groups were clustered away from the untreated control and 42.8% of the cumulative variance was explained among the 6 different treatments. A clear separation between the control and compound treated samples was observed, however, data for compounds WD30030, WD10461

and WD20542 were not well differentiated from each other, indicating an overlapping impact on the *Chlamydomonas* metabolome, while compounds WD10784 and WD20067 were well separated from the other 3 compounds and from each other. The corresponding PCA loading plots of the metabolite data are given in Supplemental Fig. S6A. The normalized and pareto scaled data was subjected to univariate analysis and fold change was calculated. Metabolites that have p value < 0.05 in at least one treatment/control ratio comparison were highlighted in red in the loading plot.

The pareto scaled data was further subjected to Partial Least Square Discriminate Analysis (PLS-DA) analysis to investigate deep differences between the treatment groups and untreated control cells to find potential biomarkers for discriminating the effect on metabolism due to specific treatments (Fig 7B). The score plot showed good fit to model as the untreated control group was well separated from the treated samples. The model demonstrated good predictive ability with a $R^2Y(cum)$ of 0.956 and $Q_2(cum)$ of 0.865. The S-plot (Supplemental Fig. S6B) and the variable importance for projection (VIP) plot of the OPLS-DA model (Fig. 7C) was used to select the variable responsible for the group separation. Based on the VIP scores (deduced using www.metaboanalyst.ca web-tool and the S-plot generated from the OPLS-DA model using muma R package), the top 20 metabolite biomarkers were illustrated to demonstrate biochemical signatures could be identified to show impact by the different compounds (Fig 7C). Further, a heatmap, generally used for unsupervised clustering, was also constructed based on the top 50 metabolites identified via ANOVA as having a $p < 0.05$ (Fig 8). Concordance and differences between compound treatment effects on metabolites identified are illustrated in a Venn diagram (Fig. 8B). A complete list of the identified metabolites and comparison between treatments (Log2-fold change values) are given in Supplemental Table S4 and the raw intensities are given in Supplemental Table S5. Of the 125 identified, 33 metabolites were not significantly changed by any treatment condition, while 15 that were significantly different from control levels were common to all treatment groups. The fewest number of significant changes in metabolite levels, 36/125, were measured for cells treated with WD20067. The KEGG brite hierarchy was used to classify the different metabolites (Fig. 8C) and suggested that 11% contain phosphates, 12% were amino acids and 6% were biogenic amines. Fatty acids and carbohydrates contributed 7% of the total profiled metabolites. The largest number (38%), however, remain as unidentified.

Metabolite analysis provided valuable information on similarities and differences in central carbon and amino acid metabolism for the 5 compounds assessed (Table 4, Fig. 9 and Fig. 10). Relative levels of key metabolites in glycolysis, gluconeogenesis, the TCA/glyoxylate cycles and photorespiration/carbon fixation were different between compound treated and control samples (Table 4). Glucose levels were elevated when cells were treated with compounds WD30030 and WD20542 but were not significantly different from control values for other compounds. Glucose-6-phosphate (G-6-P), a metabolite of glycolysis and a potential substrate for starch synthesis accumulated to varying levels with compound treatments. In general, the levels of starch accumulating in response to compound treatment roughly reflected the concentration of G-6-P with compound WD10784 inducing both highest levels of this substrate and starch product (Table 4 and Fig. 5A). In contrast, compound WD20067 induced the lowest accumulation of G-6-P and slightly elevated starch levels. Additional metabolites of glycolysis, gluconeogenesis and the Calvin cycle that were identified included phosphoenolpyruvate (PEP) and glycerol-3-phosphate (3-PG). PEP levels were significantly lower in cells treated with any of the compounds compared with control. The same was true for 3-PG with the exception of cells treated with WD20067, which was equivalent to controls. In contrast, levels of the glycolytic intermediate fructose-6-phosphate (F-6-P) also derived from G-6-P were elevated but to varying extents. Very high levels were achieved in cells treated with WD10784 (360-fold), modest increases were observed after treatment with WD 30030 and WD20542 (17- and 34-fold, respectively), while WD20067 increased this metabolite slightly (2.5-fold). Fructose-1,6-bisphosphate (F-1,6-P), in contrast, was significantly reduced by treatment with each of the compounds perhaps due to efficient conversion to glyceraldehyde 3-phosphate (G-3-P) and dihydroxyacetone phosphate (DHAP), which can feed into the Calvin cycle to regenerate Ru-1,5-P.

Four metabolites of the TCA cycle were identified and compared after compound treatment. Isocitrate concentrations were somewhat elevated by all compounds but differences were only statistically significant for WD30030, WD10641 and WD20542. Alpha-ketoglutarate levels were not significantly different for WD30030, WD10461 or WD20542 but were slightly elevated by WD10784 and WD20067. This TCA cycle intermediate is formed by the decarboxylation of isocitrate and results in the net loss of one carbon as CO_2. Succinate can be formed by a second decarboxylation or when carbon loss is bypassed through the formation of

glyoxylate. While glyoxylate was not identified in these analyses, succinate was identified and its levels were significantly higher than controls under all compound treatments, perhaps reflecting the anabolic state of the cells treated with compound to allow net assimilation of carbon and storage of lipid and starch. Fumarate levels were also slightly higher after treatment with WD30030 and WD20542. While malate and oxaloacetate were not identified in these experiments it was noted that oxalic acid, an OAA metabolite was highly elevated in all treatments, possibly due to increases in the substrate OAA. Citrate is a critical TCA cycle intermediate that is also a substrate for lipid synthesis when energy demands of the cells have been met, and was previously noted as elevated in nitrogen deprivation of *Chlamydomonas* (Wase et al., 2014). Citrate was not identified in our non-targeted analysis so it was measured directly (Supplemental Table S6B). Two compounds, WD30030 and WD20067, increased citrate levels significantly by about 25% while the 3 other compounds had no significant effect.

Erythrose-4-phosphate (Er-4-P) is a key intermediate shared by the pentose phosphate pathway and the Calvin cycle. It also serves as a substrate in the biosynthesis of the aromatic amino acids tyrosine, phenylalanine, and tryptophan. Er-4-P was significantly reduced by treatment with each compound except WD10784. Ribulose-5-phosphate (Ru-5-P), ribulose-1,5-bisphosphate (Ru-1,5-P) , and xylulose-5-phosphate (X-5-P), also metabolites of the Calvin Cycle, were significantly elevated by all compounds with the exception of WD10461. The latter only elevated accumulation of X-5-P to a small, but significant extent and did not influence the other two metabolites. Taken together, these data indicate the Calvin Cycle remains active in compound treated cells compared with controls. This results in the net gain of carbon as lipid, and for some compounds starch as well.

Twelve amino acids were identified in this metabolite assessment, as well as 12 metabolites involved in amino acid synthesis or degradation (Table 4 and Fig. 10). There was, in general, an elevation of most amino acids identified and some substrates required for their synthesis. However, between compounds there were different patterns of impact on the levels of specific amino acids. It was notable that compound WD30030 increased the abundance of 9 of 12 amino acids and 8 substrates or metabolites of amino acid synthesis or degradation. Alanine and valine, each derived from pyruvate, were elevated 20-fold or more when cells were treated with this compound. In contrast treatment with compounds WD10784 or WD10461 had more limited impact on most of the amino acids evaluated.

Citrulline levels were very highly elevated compared with controls after each compound treatment and this led, correspondingly, to elevated arginine levels. Chorismate, an intermediate in the synthesis of the aromatic amino acids, was elevated 30- to 40-fold by treatment with compounds WD30030, WD10461 and WD20542 but was only slightly elevated by WD10784 and was not increased by WD20067 treatment. Tyrosine levels followed a similar pattern, as expected. Tryptophan and phenylalanine, however, were not identified in our data sets. Sarcosine an intermediate and degradation product involved in glycine metabolism was elevated by all compounds except WD20067. Markedly reduced by most compound treatments were homocysteine, cysteic acid, and homoserine, each involved in threonine and methionine production. Aminoadipic acid, a catabolite of lysine, was highly elevated by WD10784 treatment and to a lesser extent by the other compounds.

Metabolites involved in nucleotide metabolism were impacted to varying extents by the different compounds. Adenine levels were not significantly different from controls for any compound, whereas guanine and uracil levels were significantly decreased. Thymine levels were only significantly decreased in cells treated with WD30030; other compounds had no effect. Deoxyadenosine accumulated to 95-fold control levels in cells treated with WD20067, while the other compound treatments did not significantly alter levels of this compound.

Additional metabolites identified and compared that are of interest included phytol, a metabolite of chlorophyll. As expected, since photosynthetic pigment levels were maintained, abundance of this compound was not significantly different between treatment and control samples. A compound implicated in plant and root growth, 5-hydroxy-tryptamine(Akula et al., 2011), was significantly elevated by all compound treatments. Most notably, the levels of a flavonoid apigenin, suggested for use in treatment of some cancers, accumulated 2,000-fold after WD30030 treatment, 1,200-fold by WD10461 and WD20542 and to somewhat lesser extent by the other 2 compounds. Thus, these lipid-activating compounds may also be of value in producing this important compound as a coproduct.

Small molecule activators of lipid accumulation function in other algal species

Previous work has demonstrated Nile red fluorescence is a useful measure of neutral lipid droplet accumulation (Greenspan et al., 1985; Chen et al., 2009). In the current work, NFC

values correlated well with measurements of fatty acid levels (Table 1), TAG and GL (Figure 6) quantification in *Chlamydomonas* for compounds WD10784, WD10461, WD30030, WD20542, and WD20067. Therefore, estimations of NFC were used to evaluate whether or not the compounds were also effective in stimulating lipid body production in three additional fresh water algae, *C. vulgaris* UTEX395, *C. sorokiniana* UTEX1230, and *T. alterns* UTEX2453 that represent potential feedstock candidates for biofuel production (Mallick et al., 2012; Rosenberg et al., 2014). These green algae are fast growing, have short doubling times in heterotrophic media and can accumulate high levels of lipids during stress (*e.g.* up to 56% and 39% for UTEX 1230 (Wan et al., 2012) and UTEX 395 (Rosenberg et al., 2014), respectively). Growth of the cells with compound was comparable to *Chamydomonas* and as shown in Table 5 and Supplemental Table S2, the selected compounds increased lipid accumulation in these microalgal species as well.

DISCUSSION

Most platforms currently used to increase lipid accumulation for biofuel and bioproduct production in algae employ abiotic stress, which also limits biomass accumulation. Using high throughput methods, we screened 43,783 compounds and selected 243 small molecule activators in *Chlamydomonas reinhardtii* that increased lipid body accumulation and maintained continued growth over 72 h thus fulfilling two important criteria in advancing algae for use in next generation biotechnology applications. The compounds were classified according to structural similarities into 5 subgroups. Biochemical characterization of 15 representatives verified the stimulation of lipid body accumulation and elevated total fatty acid abundance for each, and also established unique impacts on starch accumulation and plastidic components. Further analyses using metabolomics approaches demonstrated 5 lipid activators from various structural families had separable impacts in terms of cellular metabolic processes. In general, metabolite profiles were similar between WD10784 and WD10461 by comparison with WD30030 and WD20542, while WD20067 displayed a pattern distinct from the other 4 compounds. WD20067 is of particular interest since this compound induced very high TAG accumulation, only slightly increased starch levels, and had the least impact on polar metabolites.

Among non-polar metabolites, all compounds tested resulted in increased levels of TAGs. Importantly, for 4 compounds, galactolipids were essentially equivalent to wild-type indicating these membrane lipids were not a major source of acyl chains in the TAGs as occurs in many stress conditions (Hu et al., 2008; Urzica et al., 2013; Allen et al., 2017) or with treatment with the small compounds brefeldin A (Wase et al., 2015) or fenpropimorph (Kim et al., 2015). In contrast, treatment with WD20067, decreased galactolipid content to about 25% of control values, which is more similar to nutrient deprivation (Goncalves et al., 2013; Urzica et al., 2013; Allen et al., 2017).

In general, WD30030 maintained carbon flux through glycolysis, the TCA cycle, Calvin cycle and OPPP leading to increased levels of a number of amino acids and TAG with only a moderate increase in starch synthesis. By contrast, WD10784 increased storage of both TAG and starch, possibly due to very high levels of G-6-P compared to controls or other compounds tested. Of note were the reduced glucose levels when cells were treated with WD10784 or WD10461; this was in contrast to treatment with WD3003 and WD20542, which accumulated glucose to levels significantly higher than controls perhaps reflecting slower conversion of intermediates to starch. Bolling and Fiehn assessed metabolite changes when *Chalydomonas* was deprived of iron, nitrogen, sulfur or phosphate (Bolling and Fiehn, 2005). Among these conditions only sulfur starvation resulted in elevated G-6-P levels (3.2-fold) and no condition elevated glucose levels above control values.

While treatment with WD10784 induced lipid and starch accumulation, there was a commensurate decrease in total biomass and cultures were moderately chlorotic corresponding to loss of carotenoids and chlorophylls. In contrast, cells treated with WD30030 accumulate large quantities of lipids (Fig. 6 and Table 1; Supplemental Table 6A) with no effect on starch or pigments (Fig. 4), and little impact on growth. Twice as many polar metabolite concentrations were reduced as a consequence of WD10784 treatment, and 25% fewer were increased compared with WD30030. Many of these measured differences in metabolite levels between compound treatments were attributable to the WD10784-mediated reduction of some amino acids and amino acid precursors, and higher concentrations of the same metabolites measured after WD30030 treatment. Thus, these two compounds offer contrasting metabolite profiles useful to dissect pathway mechanisms and components leading to TAG and/or starch storage. In this regard, WD10784 treatment affected changes in amino acid metabolism similar to that which

492 occurs in abiotic stress (Bolling and Fiehn, 2005). Future physiological and omics analyses of
493 similarities and differences between a “stressful” compound like WD100784 and a “non-
494 stressful” compound like WD30030 or WD20067 are warranted to provide additional
495 mechanistic details of compound activities.
496 The metabolite profiling data provided broad coverage for many intermediates of
497 glycolysis, gluconeogenesis, TCA and glyoxylate cycles, as well as the intersecting Calvin cycle
498 and oxidative pentose phosphate pathway (OPPP) (Fig. 9). These experiments profiled cells
499 grown myxotrophically on acetate using both photosynthesis and the exogenous carbon source
500 via the Calvin and glyoxylate cycles, respectively (Chapman et al., 2015). Acetate can enter
501 anabolic pathways to produce lipid and starch for storage at multiple points relieving the
502 necessity of employing photosynthesis solely for this purpose. The chloroplast is the site of fatty
503 acid synthesis using both fixed CO_2 and exogenously supplied acetate, so maintaining the
504 integrity of this organelle is important to the success of the compounds that function to channel
505 substrates to fatty acid synthesis and lipid.
506 The abundance of key metabolites of glycolysis and the Calvin cycle including G-6-P, F-6-
507 P, and X-5-P were significantly elevated for all compounds with variations in the scale of
508 impact. These pathways operate in parallel sharing metabolites and providing reducing
509 equivalents for anabolism. The anabolic state of compound-treated cells was apparent from the
510 higher abundance of many amino acids, lipids and starch. This is in direct contrast to nutrient
511 starvation conditions such as nitrogen deprivation where starch and lipid accumulate at the
512 expense of amino acids, proteins and nucleic acids (Bolling and Fiehn, 2005; Hu et al., 2008;
513 Cakmak et al., 2012; Wase et al., 2014). Storage of lipids and starch further require substrates
514 and reducing equivalents supplied by the OPPP and Calvin cycle. The activities of these
515 pathways were reflected in elevated levels of Ru-5-P, Ru-1,5-P, and X-5-P with treatment using
516 most compounds. Treatment with WD10461 was distinctive as levels of these intermediates did
517 not significantly differ and in the case of X-5-P were only slightly elevated.
518 The unique state of cellular metabolism with compound treatment was further reflected in
519 the elevation of many amino acids and metabolites that are substrates for their synthesis (Fig.
520 11). In contrast, nucleotide bases, while maintained at levels comparable to controls under most
521 treatments, did not increase in parallel with the storage of lipid and starch and amino acids.
522 Thymine and adenine levels were approximately equal to control values, while levels of guanine,

guanosine and the metabolite xanthosine were significantly reduced. Only deoxyadenosine and deoxyinosine monophosphate were increased in abundance with some compound treatments. It is unclear at this time what, if any, linkages there are between the different compound treatments on nucleotide levels and relationships to cell growth or accumulation of TAG or starch.

A consideration in assessment of the metabolic adaptations to these compounds is how to determine levels of stress response. In an attempt to minimize stress, we selected only compounds that allowed growth and did not become chlorotic over 72 hours of treatment. Metabolite analyses did not show an increase in nicotianamine and did not identify trehalose, two compounds that accumulate in nitrogen starved cells and are considered to be protective (Wase et al., 2014). On the other hand, accumulation of the antioxidants ascorbic acid, apigenin and kaempferol after treatment with some compounds might be indicative of oxidative stress. Indeed, in mammalian cells accumulation of lipid above normal levels in non-adipose tissues is associated with dysfunction of the endoplasmic reticulum and mitochondria in a process called lipotoxicity (Unger and Scherer, 2010). It is possible that algal cells undergo the same stresses as lipids accumulate above normal levels.

In a separate report Franz and colleagues identified a different set of compounds that also increase lipid accumulation in marine green algae a subset of which also maintained growth (Franz et al., 2013). The most effective compounds increased lipid accumulation 2-fold, while most only reached 20-40% above control levels. As no metabolite or other biochemical pathway analysis for these compounds was reported, nor are they related by structure to the compounds reported herein, it is not clear if they offer divergent or overlapping mechanisms of action. It is noteworthy that apigenin was a compound tested in that library but did not induce lipid accumulation when added exogenously (Franz et al., 2013). Targeted selection and assessment of small compounds as activators of lipid accumulation have also been attempted. The compounds were chosen based on activity in other organisms and included signal transducers such as auxin and gibberellin (Li et al., 2015) and modulators of MAPK kinase pathways (Choi et al., 2015). In each case lipid storage was low, less than 25% above controls. In noted contrast, the molecules reported herein increased lipid storage to much higher levels and offer contrasting impacts on metabolite profiles and storage compound accumulation that may be exploited in the future to evaluate metabolic pathway flow that leads to useful bioproducts in algae.

CONCLUSIONS

A high throughput screening approach targeting lipid accumulation and growth in green algae successfully identified lipid activating compounds. Further chemical genetics analyses resulted in novel findings showing that lipid accumulation can be separated from severe abiotic stress pathways such as those induced by nutrient deprivation. A subset of the selected compounds stimulated lipid accumulation without depleting galactolipids, chlorophylls or carotenoids, providing strong evidence that algal cells can synthesize storage lipids by metabolic routes, which will not compromise the photosynthetic apparatus. Further, the distinct biochemical signatures associated with various compounds may be exploited to further scrutinize overlapping and divergent metabolic shifts that contribute to lipid, starch and amino acid synthesis in green algae for which understanding of gene and protein expression is relatively limited. Hence this chemical genetic approach offers unique insights into algal metabolism that are intractable at this time by classical genetic or molecular biological approaches.

The activity of TAG storage stimulating compounds identified using *Chlamydomonas*, a valuable model organism but not a useful biofuels feedstock, was also verified in 3 other algal biofuel production species. While the level of response between species and between compounds were not exactly the same for each of the 15 selected compounds, these analyses provided important verification of the induction of lipid synthesis across microalgal species. Additionally, two flavonoids under scrutiny for use as nutraceuticals and chemotherapeutics, kaempferol and apigenin, were highly elevated in compound treated algal cells (Weng and Yen, 2012; Sak, 2014; Sung et al., 2016). Apigenin reached levels more than 1,000-fold higher than controls under all compound treatments except WD10784. Similar HTS approaches may be adapted to other algal species to devise screens for additional biotechnological applications, opening the door for the production of otherwise unforeseen economically impactful compounds.

MATERIALS AND METHODS

Materials, strains and culture conditions

All chemical reagents were obtained from Sigma-Aldrich (St. Louis, MO) unless otherwise stated. Nanopure water at 18 Ohms was obtained from Milli-Q Millipore (Millipore, Milford, MA). Clear transparent 384-well and 96-well plates used for growing cells and black-walled flat bottom plates for fluorescent assays were obtained from BD Falcon (BD Biosciences, San Jose, CA).

Chlamydomonas reinhardtii CC125 wild type strain was obtained from the Chlamydomonas Resource Center (University of Minnesota, Twin Cities, MN). Cells were routinely maintained on tris-acetate phosphate (TAP) agar plates at 25°C with a photon flux density of 54 μmol $m^{-2}s^{-2}$ (Harris, 2009). For the screening, a sterile loop of cells was introduced to a 250 mL Erlenmeyer flask (100 mL TAP media) with a rubber stopper for facilitating gas exchange and grown for 72 h in a shaking incubator and the same temperature and light settings. When N limitation was required to induce lipid accumulation, ammonium chloride was omitted from the TAP formulation. For screening, cells were harvested in log phase, rinsed either in N-replete or N-deficient TAP media, and then dispensed at low cell density (5×10^5 cells/well) to 384-well microtiter plates (f.vol. 50μL).

Chemical library screening

The library of 43,736 compounds used for screening algae for lipid accumulators was obtained from ChemBridge corporation (http://www.chembridge.com). Over 60 proprietary chemical filters (including Lipinski's rule of 5) and Daylight Tanimoto similarity measures were used to assure structural diversity, and drug-likeness of compounds for the selected collection. The compounds were selected based on 3D pharmacophore analysis to increase diversity and coverage of chemical space and guided by Lipinski's rule of 5 (Lipinski et al., 1997). Compounds from 10 mM stock were transferred to the 384-well plates for screening using an ECHO 555 (Labcyte, Sunnyvale, CA) to give a final concentration of 10 μM. For each plate, two columns were reserved for the positive (TAP media without nitrogen; N-) and negative controls (complete TAP media; N+) of lipid accumulation. N+ cultures also served as a positive control for growth and the N- cultures as negative control for growth. To test the effects of the compounds on both growth and lipid accumulation, cells from a log phase culture were

harvested, rinsed 3 times with N+ media, then resuspended to yield 1 x 10^5 cells in 50 µL. To each well containing compound, 50 µL cell suspension was dispensed for assessment. On each plate, the N- controls were prepared from the same starter cell culture except that an aliquot was rinsed 3 times in N- media and dispensed in same media to wells of the first column of each plate at a cell density of 5 X 10^5 cells in 50 µL. The N- cultures doubled approximately once during the 72 h culture period, while the N+ cultures reached approximately 1 X 10^6 cells at the end of the 72 h incubation period. The cell samples in the second column of each plate received the vehicle, DMSO, alone to serve as the N+ control.

Once filled, the plates were sealed using gas permeable adhesive film (BreathEasy, Diversified Biotech) and were cultured under cool white fluorescent lights (approximately 50 µmol m-2s-2) at room temperature on racks. Plates were shaken once per day in a Titermax shaker (Heildolph North America, Elk Grove, IL) for 5 min at maximum speed. After 72h, plates were read at OD_{600} nm to assess growth. The average OD_{600} for N- control wells over all plates was 0.46 ± 0.03 and for N+ wells was 0.41 ± 0.04.

After 72h of incubation with compound, Nile Red stain (30 µM f.c. in DMSO) was added to each well using the ECHO 555 to identify neutral lipid droplets (Greenspan et al., 1985; Chen et al., 2009). Plates were incubated for 60 min at 37 °C in the dark. After incubation, cells were mixed in a Titermax shaker, maximum speed for 5 min and fluorescence recorded using a Synergy BioTek Neo multimode reader (BioTek Instruments, Winooski, VT) in fluorescence mode at 485/590 Ex/Em.

To visually assess lipid droplets within cells, an aliquot of cells after staining with Nile red were imaged with an Olympus IX81 inverted confocal laser scanning microscope (Olympus Scientific Solutions Americas Corp., Waltham, MA) using FloView v5.0 software (100X; oil immersion). Details of emission and excitation wavelengths used are given elsewhere (Wase et al., 2014).

Employing both the final OD_{600} and AFU for Nile Red a fold-change (NFC) was calculated as:

$$\mathrm{NFC} = \frac{(Sample\ NR\ intensity\ )/(Control\ NR\ intensity)}{(OD\ Sample)/\ (OD\ Control\ )}$$

Selection of primary hits

A compound was considered active in *C. reinhardtii* if the Z' factor of the plate was > 0.5 and the Nile Red AFU ratio for compound/control was > 2.5-fold. Compounds that passed the first screening were cherry picked from the library and retested for confirmation of growth and lipid induction using an 8-point titration curve from 0.25 to 30 μM. Endpoint readings were taken after 72 h at OD_{600} and Nile Red staining was used to assess lipid accumulation. Additionally, image capture on a BD pathway^{TM} high content Bioimager (BD Biosciences, San Jose, CA) at 10X magnification was performed as a visual confirmation of lipid body accumulation (data not shown). The fluorescent lipid bodies appeared as a speckled phenotype within the cells. This phenotype was reconfirmed for the final set of 243 compounds showing ≥ 2.5 fold induction at one or more concentrations using a Nikon Ti-inverted microscope (Nikon Corp., Tokyo) equipped with Photometrics CoolSNAPHQ2 camera (1392 X 1040 array with14-bit digitization for 16,000 grey levels capability) (Photometrics, Tuscon, AZ).

Chemoinformatics

For the final subset of 243 hit compounds selected from the primary screen, PubChem fingerprints were calculated using the ChemViz plugin in Cytoscape v3.2 (Wallace et al., 2011). Chemicals with a similarity Tanimoto value ≥ 0.7 (1.0 being identical) were used for similarity network generation. Further results from the re-confirmation studies were used to draw pie charts on the nodes, and lipid accumulation measured using NR fluorescence values from the 30 μM treatment for each compound were used to determine node size. For identification of molecular framework / scaffold and structural clustering, the structures for the 243 compounds and the corresponding Nile Red fold change values at 8 concentrations were imported into Scaffold Hunter (Wetzel et al., 2009).

Photosynthetic pigment analysis

Analysis of photosynthetic pigments including chlorophyll a, b and total carotenoids was conducted as reported previously (Wase et al., 2015). Briefly, cultures (50 ml) were grown with

or without compound in triplicate at the specified final concentrations for 72h at 25˚C with shaking in a New Brunswick Innova® 43 incubator under a photon flux density of 54 μmol $m^{-2}s^{-2}$. Cells were harvested, media removed and samples lyophilized overnight at -50°C under vacuum. To 5 mg dry biomass, 1 mL of 100% methanol was added, cells were homogenized and pigments extracted at 4°C for 2 hours. Samples were clarified by centrifugation at 14,000 x g for 5 min and then the supernatant was read at 666, 653 and 470 nm using a UV-visible spectrometer (BioMate 6; Thermo Scientific, Waltham, MA). Calculations for chlorophyll a, b and total carotenoids was computed as given elsewhere (Lichtenthaler and Wellburn, 1983).

Measurement of starch, citrate and protein levels

Levels of starch were determined using the Starch Assay kit (Sigma) according to the manufacturer's instructions. Briefly, triplicate cultures (100 ml each) were grown either with compounds at the specified final concentrations or with vehicle (DMSO) in triplicate for 72h as above. After 72h, cells were recovered, media removed and cells were freeze-dried overnight. Five milligrams of freeze dried powder was resuspended in 1 mL 100% methanol and incubated at 4 °C to extract the pigments. The colorless pellet was processed as per manufacturer's instructions. Absorbance of the final reaction mixture was measured at 340 nm.

Intracellular citrate levels were determined using Citrate assay kit (Sigma Catalog Number MAK057) according to the manufacturer's instructions.

Total protein levels after treatment were measured for cells grown with or without compounds using the BioRad DC reagent kit (Bio-Rad Corp., Hercules, CA) according to the manufacturer's protocol.

Assessment of compound efficacy in additional green algal species

To evaluate the activity of the compounds in additional algal species, we employed *Chlorella sorokiniana* UTEX 1230, *Chlorella vulgaris* UTEX 395 and *Tetrachlorella alterens* UTEX 2453. Briefly, cells were maintained on TAP plates and pre-grown in 100 mL liquid culture for subsequent passage. Cells were plated at a low density (5 x 10^5 cells/well) in a 96-well plate (200 uL f. vol.) and the compounds were added at 8 different concentrations (0.65 to

50 µM). Growth was continued under light and the cell suspensions were mixed by shaking once every 24h. After 72h, Nile Red was added to f.c. 30 µM, and plates were incubated in the dark at 37°C for one hour. Nile Red fluorescence was measured as described above. Three independent experiments were run, each in triplicate. Normalized fold change values were calculated as the results for compound treated samples compared to control (N+) samples. Data is reported as mean of three independent experiments (sampled in triplicate) ± standard deviations (SD).

Lipid analysis

For identification and quantification of fatty acids after compound treatment, cells were harvested from 100 ml of control or compound treated culture (f.c. 30 uM) after 72 h growth, lipids were extracted using the methyl tert-butyl ether (MTBE) method and fatty acid methyl esters were analyzed by GC-MS as detailed in the Supplemental Methods S1. Data were presented as the mean ± standard deviation of 3 experiments.

Analysis of triacylglycerides (TAG) and galactolipids (GL) by LC-MS/MS is detailed in Supplemental Methods S1 under the headings: Targeted analysis of complex lipids from compound treated cells and Quantification of complex lipids by LC-MRM/MS.

Metabolite extraction, analysis and data processing

Metabolites were extracted from freeze dried cells using MeOH:CHCl3:H_2O (5:2:2; v/v/v; pre-cooled at -20°C). The extracts were processed and trimethylsilylated as describe in Supplemental Methods S1. GC-MS data acquisition and analysis of chromatograms was performed as previously reported (Wase et al., 2014). Details of the data analysis strategy are presented in the Supplemental Methods S1 under the heading: Metabolite data preprocessing and statistical analysis.

Statistical assessment and chemoinformatics analysis of compounds

All experiments were done at least in triplicate, and the results were presented as the mean ± standard deviation between experiments. The differences between compound treated and controls were analyzed by Student's t-test using GraphPad Prism V6.0. Statistical significance

was accepted at a level of $p < 0.05$. Primary screening data was analyzed using HCS-Analyzer an open source application for High Content screening (Specht et al., 2015) and chemoinformatics analysis was done using bioconductor ChemmineR package (Schaffer, 2003) or Tibco Spotfire Lead Discovery. Structural rendering of the compounds was done using ChemDraw Professional 14 suite (PerkinElmer). Compound similarity network generation was performed using Cytoscape ChemViz plugin (http://www.cgl.ucsf.edu/cytoscape/chemViz/) and molecular framework/scaffolds were identified using Scaffold Hunter (Wetzel et al., 2009).

ACKNOWLEDGEMENTS

We gratefully acknowledge the Nebraska Center for Energy Science Research (NCESR) and the National Science Foundation (NSF-EPSCoR, EPS-1004094 and 1264409 and CBET 1402896) for support that made this work possible. We also gratefully acknowledge the Kansas University High Throughput Screening Center where the HTS was performed under the direction of Dr. Anu Roy with the technical assistance of Peter McDonald.

Accession Numbers

Data from the primary screening of 43,715 compounds that induce lipid accumulation in *Chlamydomonas reinhardtii* can be found in the PubChem data repository under BioAssay record number 115937. Data from the confirmatory screen evaluating 367 potential bioactive compounds can be found in BioAssay record number 1159536.

SUPPLEMENTAL MATERIALS

Supplemental Material 1 includes:

Supplemental Methods S1: Fatty acid methyl esters analysis of compound treated cells; Targeted analysis of complex lipids from compound treated cells; Quantification of complex lipids by LC-MRM/MS; Metabolite extraction and analysis by GC-MS

Supplemental Figure S1. Experimental workflow in the high throughput screening.

Supplemental Figure S2. Representative plate D088 showing log2 NR fold change intensity.

Supplemental Figure S3. Signal distribution in controls and compound treated samples.

Supplemental Figure S4. SSMD (Strictly standard mean difference) analysis of 124 plates in the primary screen.

Supplemental Figure S5. Heatmap profile showing lipid induction in 243 hit compounds from the confirmatory screen.

Supplemental Table S1. Fold change in fatty acid species from cells treated with selected compounds.

Supplemental Table S2. Lipid accumulation is increased in a dose dependent manner by15 selected hit compounds in 4 algal species (n=3).

Supplemental Material 2 includes:

Supplemental Table S3. Data from the confirmatory screening of 367 compounds

Supplemental Table S4. Log2 Fold Change values for metabolites from compound treated versus control cells

Supplemental Table S5. Raw intensities for metabolites from compound treated versus control cells

Supplemental Table S6. A. Starch and lipid data after compound treatment used to calculate fold change values. B. Citrate levels in compound treated cells.

FIGURE LEGENDS

Figure 1. Summary of results of high throughput screening. A, Z-factor calculation for each of 124 plates totaling 43,736 compounds. The average Z' value was 0.78 ± 0.08 with a coefficient of variation (CV) of 14.4%. B, Growth measured as OD_{600} in the presence of compound after 72h. The average of the N+ control cells was 0.41 ± 0.04. C, Lipid accumulation measured as relative fluorescence after Nile Red (NR) staining of cells treated with compound relative to cells treated with vehicle (DMSO). D, Confirmation of hits and dose response. Data for 243 compounds are shown fitting the concentration response curve (from 0.25 μM to 30 μM) to lipid accumulation. The scale bar represents the relative fold change of treatment to control (N+).

Figure 2. Structural comparisons of hits from the primary screen. A, Network view of lipid accumulating small molecules. All small molecules identified through the primary screen and verified using an 8-point dose response curve were clustered according to their Tanimoto similarity score. Each node represents a unique small molecule. Edges represent the structural similarities at a Tanimoto score cuttoff of 0.70. Data for the relevant compound at 30 μM (red), 15 μM (green) and 10 μM (blue) are mapped in a pie chart. The node size represents the fold change of each chemical at the 30 μM concentration. A small portion of the network is magnified to show clustered compounds having structural similarities. B, Clustering analysis of active compounds using Ward's linkage method. Distance was calculated based on Tanimoto coefficient and Estate bit fingerprints were used for similarity calculations. One of the clusters was highlighted showing the admantane moiety. Note some of the compounds are presented as salts of HCl; 2 HCl molecules indicate chiral enantiomers.

Figure 3. Lipid body accumulation in *C. reinhardtii* induced by diverse compounds. Compounds are grouped according to their structural similarities as described in the text. Cultures were treated with 10 μM compound and the corresponding lipid accumulation was visualized using confocal microscopy after 72h in culture.

Figure 4. Growth of cells and accumulation of protein during compound treatment. A, Cells were treated with 30 μM of the specified compounds as indicated and OD_{600} was monitored over 72h (n=3; ± SD); B, after harvesting, total protein levels were measured per 10^6 cells.

817 Bar height indicates the mean of 3 biological replicates (n=3 ± SD). Significance of
818 difference in the levels of total protein was assessed using ANOVA to compare the treated
819 samples to controls (* $p<0.05$; **, $p< 0.01$; ***, $p< 0.001$).
820
821 **Figure 5.** Assessment of cellular macromolecule accumulation after treatment with selected
822 compounds for 72h. A, Total starch; B, Total carotenoids; C, Chlorophyll a; and D,
823 Chlorophyll b. Bar height is the mean of 3 independent experiments (± SD). The controls
824 were values obtained for cultures treated with the vehicle DMSO. ANOVA (JMP v11) was
825 applied to determine the significance of differences in the levels of total protein as compared
826 to untreated control cells (N+) (* $p<0.05$; **, $p< 0.01$; ***, $p< 0.001$).
827
828 **Figure 6.** Identification and quantification of complex lipids by LC-MS/MS. A, triglycerides
829 (TAG) B, galactolipids (GL) and C, relative quantities of TAG and GL as indicated. Height
830 of the bar is the mean of the absolutely quantity of the measured lipid species and error bars
831 give the S.E.M (* $p<0.05$ relative to control; n=3). The relative fold change compared with
832 control values are listed below each bar for A and B.
833
834 **Figure 7.** Univariate and multivariate analysis of the GC-MS metabolites. A, PCA of
835 primary metabolites/features of compound treated and untreated control samples. Control
836 (black), WD30030 (red), compound WD20542 (cyan), compound WD10461 (blue),
837 compound WD20067 (green) and compound WD10784 (pink). B, Partial Least Square-
838 Discriminate Analysis (PLS-DA) of the data for better separation of the samples to identify
839 features that are responsible for differentiation in the treatment. C, Top 20 metabolites with
840 significantly different abundance between compound treatments based on the VIP projection
841 deduced using Metaboanalyst web tool (http://www.metaboanalyst.ca).
842
843 **Figure 8.** Summary of metabolite profiling experiments. A, Heatmap showing the metabolite
844 abundance profiles of compound treated versus control cells. The expression levels of the top
845 50 metabolites selected after applying ANOVA $p < 0.05$ are illustrated. B, Venn diagram
846 showing the unique and common differentially changed features/metabolites in different
847 compound treated metabolomes. The numbers of peaks that were not significantly changed
848 (33) are shown at the bottom right. C, Metabolite peaks generated after peak picking and
849 deconvulation, were identified using the MassBank and GOLM metabolome libraries. For

each identified feature, a KEGG compound code was assigned as per KEGG brite and classified according to their biological role.

Figure 9. Pathway map representing the impact of various compounds on carbon metabolism. Red bar indicates significantly increased levels of metabolites in compound treated samples relative to controls; blue indicates significantly decreased levels of metabolites in compound treated samples relative to controls; and white indicates no significant difference between treated and control samples. For quantitation of changes see Table 4 and Supplemental Information 1 Tables S4A and S4B.

Figure 10. Pathway map indicating the impact of various compounds on amino acid biosynthesis. Red bar indicates significantly increased levels of metabolites in compound treated samples relative to controls; blue indicates significantly decreased levels; and white indicates no significant difference between treated and control samples. For quantitation of changes see Table 4.

866 **Table 1.** Identification and quantitation of fatty acid species from cells treated with selected compounds.

Group	Compound	C16:0	C16:1 *cis Δ9*	C16:3 *cis Δ 7,10,13*	C16:4 *cis Δ 4,7,10,13*	C18:0	C18:1 *cis Δ 9*	C18:2 *cis Δ 9,12*	C18:3 *cis Δ 5,9,12*	C18:3 *cis Δ 9,12,15*	Total_FA	p-value
	Control	2.76 ± 0.05	0.43 ± 0.02	0.44 ± 0.05	1.11 ± 0.09	0.37 ± 0.10	0.52 ± 0.19	0.40 ± 0.07	0.29 ± 0.02	2.18 ± 0.43	8.50 ± 0.75	
1	**WD40844**	10.33 ± 0.77	0.48 ± 0.04	0.45 ± 0.05	1.89 ± 0.17	1.31 ± 0.09	7.80 ± 0.72	4.01 ± 0.40	1.91 ± 0.20	2.39 ± 0.19	30.57 ± 2.62	<0.0001
1	**WDTHQ130**	9.20 ± 0.34	0.56 ± 0.04	0.50 ± 0.03	2.07 ± 0.03	1.31 ± 0.04	7.35 ± 0.17	3.92 ± 0.08	2.40 ± 0.04	2.10 ± 0.07	29.42 ± 0.82	<0.0001
1	**WD40157**	4.49 ± 0.25	0.30 ± 0.03	0.15 ± 0.01	0.64 ± 0.04	0.58 ± 0.01	2.57 ± 0.13	1.10 ± 0.07	0.58 ± 0.03	0.78 ± 0.02	11.20 ± 0.52	NS
1	**WD10784**	7.11 ± 0.78	0.28 ± 0.03	0.28 ± 0.03	0.78 ± 0.04	0.58 ± 0.12	0.79 ± 0.30	1.06 ± 0.43	0.52 ± 0.08	2.29 ± 0.84	13.70 ± 1.07	0.01
2	**WD10738**	13.48 ± 1.39	0.67 ± 0.07	0.40 ± 0.06	1.83 ± 0.26	1.32 ± 0.15	6.74 ± 0.97	3.39 ± 0.49	1.61 ± 0.24	2.30 ± 0.29	31.73 ± 3.90	<0.0001
2	**WD10599**	5.23 ± 0.42	0.23 ± 0.02	0.19 ± 0.02	1.05 ± 0.08	0.82 ± 0.05	3.57 ± 0.31	1.41 ± 0.14	1.39 ± 0.10	1.31 ± 0.11	15.20 ± 1.24	0.0002
2	**WD10461**	8.77 ± 1.38	0.73 ± 0.14	0.34 ± 0.06	1.41 ± 0.19	1.28 ± 0.19	6.43 ± 1.11	3.12 ± 0.56	1.28 ± 0.26	2.08 ± 0.37	25.45 ± 4.21	<0.0001
2	**WD10256**	7.05 ± 0.45	0.39 ± 0.02	0.39 ± 0.03	1.49 ± 0.09	1.04 ± 0.06	5.87 ± 0.34	2.95 ± 0.16	1.60 ± 0.09	1.57 ± 0.09	22.34 ± 1.34	<0.0001
2	**WD10264**	6.29 ± 0.13	0.57 ± 0.01	0.41 ± 0.01	1.80 ± 0.04	1.02 ± 0.02	6.14 ± 0.04	2.91 ± 0.02	1.81 ± 0.03	1.55 ± 0.03	22.50 ± 0.30	<0.0001
3	**WD30030**	10.51 ± 2.65	4.63 ± 4.06	0.43 ± 0.09	2.60 ± 0.44	1.37 ± 0.26	9.08 ± 1.88	4.33 ± 0.93	1.78 ± 0.84	2.83 ± 0.60	37.55 ± 8.02	<0.0001
3	**WD30999**	4.86 ± 0.06	0.43 ± 0.01	0.23 ± 0.01	1.01 ± 0.03	0.85 ± 0.04	4.47 ± 0.15	1.95 ± 0.06	1.01 ± 0.05	0.91 ± 0.01	15.72 ± 0.38	<0.0001
4	**WD10872**	4.67 ± 0.37	0.32 ± 0.03	0.24 ± 0.02	1.13 ± 0.08	0.84 ± 0.06	2.20 ± 1.12	1.82 ± 0.13	0.86 ± 0.03	2.88 ± 0.79	14.96 ± 1.06	0.0004
4	**WD10615**	4.27 ± 0.32	0.35 ± 0.04	0.25 ± 0.02	1.47 ± 0.10	0.68 ± 0.05	4.52 ± 0.38	1.84 ± 0.17	0.83 ± 0.07	0.86 ± 0.07	15.06 ± 1.13	0.0003
5	**WD20542**	6.58 ± 0.61	0.39 ± 0.03	0.25 ± 0.02	1.21 ± 0.07	1.12 ± 0.10	5.12 ± 0.41	2.55 ± 0.20	1.22 ± 0.09	1.62 ± 0.13	20.06 ± 1.64	<0.0001
5	**WD20067**	8.25 ± 1.58	0.43 ± 0.09	0.29 ± 0.07	1.27 ± 0.29	1.19 ± 0.19	5.30 ± 1.07	2.58 ± 0.56	1.24 ± 0.32	1.86 ± 0.34	22.41 ± 4.48	<0.0001

867

868 Values are the mean of three experiments ± SD given in µg/5x10^6 cells. Cultures (100 ml) were treated with 30 µm of the indicated compound for 72 hr except WD10784 where
869 the dose was 10 µM. Significant changes in the total FA levels for compound treatment relative to control (vehicle treated) samples were determined using student's t-test (*p*-value;
870 n=3).

871 **Table 2.** Classification of identified metabolites
872
873

Metabolite class	Total unique metabolites
Standard amino acids	15
Phosphorylated compound	14
Fatty acids*	9
Carbohydrates and sugars	9
Nucleosides	7
Biogenic amines	7
Carboxylic acid	5
Cofactors	1
Vitamins	2
Unclassified	8
Unknown	48

874 *Only those FA that were identified by GC-MS in the polar extract
875

876

877 **Table 3.** Summary of differences in abundance of the 125 metabolites after compound
878 treatment. Significantly changed metabolites were identified by applying $p < 0.05$ and log2
879 fold change = 1.
880
881

	WD30030 vs Control	WD10784 vs Control	WD10461 vs Control	WD20542 vs Control	WD20067 vs Control
Lower	12	28	19	10	17
No change	68	62	71	75	89
Higher	45	35	35	40	19

882

883 **Table 4.** Polar metabolites identified and compared between controls and compound treated cells (WD30030, 030; WD10784,
884 784; WD10461, 461; WD20542, 542; WD20067, 067).

Metabolite	030/Ctl	784/Ctl	461/Ctl	542/Ctl	067/Ctl	030_pval	784_pval	461_pval	542_pval	067_pval
	Fold change Treatment/Control					*p*-value				
Glycolysis & Gluconeogenesis										
D-Glucose	6.44	**0.63**	**0.50**	3.14	1.73	**0.0001**	0.1706	0.1676	**0.0057**	0.4262
Glucose-6-phosphate	21.87	339.33	16.54	37.90	8.10	**0.0000**	**0.0000**	**0.0000**	**0.0000**	**0.0000**
Fructose-6-phosphate	16.65	359.69	5.54	33.60	2.53	**0.0000**	**0.0000**	**0.0000**	**0.0000**	**0.0138**
Fructose-1,6-diphosphate	**0.47**	**0.71**	**0.60**	**0.44**	**0.21**	**0.0000**	**0.0015**	**0.0031**	**0.0000**	**0.0000**
Phosphoenolpyruvate	**0.27**	**0.36**	**0.33**	**0.26**	**0.52**	**0.0000**	**0.0000**	**0.0000**	**0.0000**	**0.0000**
Glycerol-3-phosphate	**0.43**	**0.84**	**0.64**	**0.47**	**0.92**	**0.0000**	**0.0256**	**0.0000**	**0.0000**	0.2569
2,3-Bisphospho-glycerate	**0.41**	1.75	**0.79**	**0.46**	**0.14**	**0.0000**	**0.0051**	0.2202	**0.0002**	**0.0000**
Lactic acid	5.68	**0.14**	**0.73**	3.41	1.66	0.2193	0.2530	0.8434	0.3969	0.7486
Photorespiration/Carbon Fixation										
Erythrose-4-phosphate	**0.50**	**0.93**	**0.68**	**0.52**	**0.72**	**0.0000**	0.4176	**0.0000**	**0.0000**	**0.0004**
Ribulose-5-phosphate	3.25	6.69	**0.71**	3.20	6.64	**0.0035**	**0.0000**	0.4142	**0.0040**	**0.0000**
Ribulose-1,5-Bisphosphate	10.19	8.73	1.56	11.46	26.72	**0.0000**	**0.0000**	0.3387	**0.0000**	**0.0000**
Xylulose-5-phosphate	9.92	14.72	3.08	13.33	23.59	**0.0000**	**0.0000**	**0.0224**	**0.0000**	**0.0000**
Glycerol-2-phosphate	5.95	6.67	4.27	3.73	1.18	**0.0000**	**0.0000**	**0.0000**	**0.0000**	0.1937
TCA/Glyoxylate Cycles										
Isocitric acid	3.78	2.01	2.51	2.73	2.00	**0.0034**	0.1433	**0.0461**	**0.0263**	0.1520
αKeto-glutaric acid	**0.67**	1.68	1.16	**0.70**	1.90	0.0804	**0.0224**	0.5136	0.1106	**0.0055**
Succinic acid	4.06	5.98	3.76	3.35	5.55	**0.0000**	**0.0000**	**0.0001**	**0.0004**	**0.0000**
Fumaric acid	2.60	1.94	1.83	2.27	1.52	**0.0163**	0.1127	0.1399	**0.0394**	0.3290
3-Oxalomalic acid	**0.58**	1.41	**0.79**	**0.39**	1.38	0.2388	0.4555	0.6066	0.0508	0.4951
Oxalic acid	34.21	47.64	44.27	28.63	22.98	**0.0000**	**0.0000**	**0.0000**	**0.0000**	**0.0000**
Carbohydrate Metabolism										
Allose	1.78	**0.34**	**0.36**	1.30	1.03	**0.0072**	**0.0000**	**0.0000**	0.2192	0.9047
Galactose	2.79	**0.47**	**0.43**	1.55	1.15	**0.0001**	**0.0076**	**0.0031**	0.0794	0.5930
Myo-Inositol	2.23	2.35	2.22	3.31	2.08	**0.0000**	**0.0000**	**0.0000**	**0.0000**	**0.0000**
Tagatose	2.73	19.49	3.48	4.16	**0.95**	**0.0000**	**0.0000**	**0.0000**	**0.0000**	0.8081
Sorbitol-6-phosphate	2.16	3.24	1.45	1.84	1.12	0.0519	**0.0040**	0.3679	0.1240	0.7962
Mannitol	1.25	**0.40**	**0.44**	**0.72**	**0.61**	0.1524	**0.0000**	**0.0000**	**0.0447**	**0.0060**
Maltotriose	**0.77**	**0.06**	**0.22**	**0.16**	**0.11**	0.2165	**0.0000**	**0.0000**	**0.0000**	**0.0000**
Lactose	**0.61**	**0.05**	**0.19**	**0.01**	**0.07**	0.8621	0.3978	0.5945	0.2216	0.4616
Ribitol	**0.52**	1.17	**0.79**	**0.52**	2.11	**0.0000**	0.1758	**0.0392**	**0.0000**	**0.0000**
Galactitol	**0.60**	1.26	**0.89**	**0.57**	2.15	**0.0001**	0.0529	0.3114	**0.0000**	**0.0000**
Kestose	1.54	**0.93**	2.74	1.93	**0.39**	**0.0265**	0.7232	**0.0000**	**0.0009**	**0.0000**
Arabinose-5-phosphate	4.58	7.58	6.23	3.80	1.98	**0.0000**	**0.0000**	**0.0000**	**0.0000**	**0.0000**
Maltose	**0.69**	**0.08**	**0.34**	**0.56**	**0.75**	**0.0006**	**0.0000**	**0.0000**	**0.0000**	**0.0093**
Starch synthesis										
Indole-3-acetonitrile	2.31	2.21	2.23	2.11	2.78	**0.0000**	**0.0000**	**0.0000**	**0.0000**	**0.0000**
Maltose	**0.69**	**0.08**	**0.34**	**0.56**	**0.75**	**0.0006**	**0.0000**	**0.0000**	**0.0000**	**0.0093**
Lipid Metabolism										
Glycerol 1-phosphate	**0.74**	1.15	1.08	**0.45**	**0.69**	0.4029	0.6889	0.8350	**0.0356**	0.3204
Mandelic acid, 3,4-OH	**0.66**	**0.70**	**0.67**	**0.52**	1.41	0.0791	0.1365	0.0872	**0.0071**	0.1399

Biotin	1.07	**0.33**	**0.36**	**0.43**	1.02	0.8335	**0.0041**	**0.0053**	**0.0140**	0.9467
Isoascorbic acid	1.01	5.61	3.29	2.25	1.38	0.9643	**0.0000**	**0.0000**	**0.0038**	0.2744
Inositol-2-phosphate	2.99	4.01	3.51	2.60	1.60	**0.0000**	**0.0000**	**0.0000**	**0.0000**	**0.0000**

Amino Acid Metabolism

Alanine	21.94	4.08	**0.05**	6.11	7.25	**0.0506**	0.4024	0.1578	0.2638	0.2334
Serine	3.33	**0.56**	1.18	**0.81**	5.53	**0.0000**	**0.0371**	0.5128	0.4137	**0.0000**
Tyrosine	4.04	**0.94**	1.68	2.66	1.86	**0.0000**	0.7164	**0.0016**	**0.0000**	**0.0003**
Leucine	3.95	**0.61**	1.80	1.60	2.44	**0.0000**	**0.0017**	**0.0036**	**0.0052**	**0.0010**
Valine	20.34	89.52	51.44	32.91	23.81	**0.0000**	**0.0000**	**0.0000**	**0.0000**	**0.0000**
Glutamic acid	1.24	**0.22**	**0.34**	**0.42**	**0.96**	0.5271	**0.0008**	**0.0078**	**0.0232**	0.9110
Proline	1.96	3.10	3.16	3.02	3.25	0.0882	**0.0052**	**0.0040**	**0.0050**	**0.0040**
Arginine	6.28	24.11	12.37	7.72	11.49	**0.0006**	**0.0000**	**0.0000**	**0.0001**	**0.0000**
Histidine	1.08	**0.41**	**0.67**	**0.79**	1.14	0.7645	**0.0068**	0.1645	0.3930	0.6405
Lysine	5.10	1.13	3.01	3.83	2.27	**0.0000**	0.4961	**0.0000**	**0.0000**	**0.0000**
Threonine	2.04	**0.83**	1.59	1.90	1.89	**0.0001**	0.3394	**0.0131**	**0.0006**	**0.0011**
Isoleucine	2.67	**0.48**	1.23	2.15	1.74	**0.0001**	**0.0071**	0.3865	**0.0021**	**0.0286**
Sarcosine	5.38	17.08	14.95	4.35	**0.90**	0.0581	**0.0016**	**0.0023**	0.1004	0.9147
Phenylpyruvic acid	3.18	1.01	1.91	2.42	1.27	**0.0000**	0.9562	**0.0024**	**0.0000**	0.2621
5-Aminovaleric acid	3.55	2.20	2.17	2.17	1.83	**0.0000**	**0.0001**	**0.0001**	**0.0001**	**0.0030**
Homocysteine	**0.44**	1.10	**0.68**	**0.40**	**0.36**	**0.0100**	0.7430	0.2111	**0.0043**	**0.0025**
2-Aminoadipic acid	1.43	24.83	8.49	5.36	2.12	**0.0346**	**0.0000**	**0.0000**	**0.0000**	**0.0001**
Cysteic acid	**0.52**	**0.12**	**0.12**	**0.33**	**0.61**	**0.0038**	**0.0000**	**0.0000**	**0.0000**	**0.0358**
Shikimic acid	2.72	20.25	12.45	4.21	5.99	**0.0000**	**0.0000**	**0.0000**	**0.0000**	**0.0000**
L-Citrulline	70.98	138.09	99.38	81.02	117.92	**0.0000**	**0.0000**	**0.0000**	**0.0000**	**0.0000**
Ornithine	1.46	**0.25**	**0.54**	1.11	1.01	0.1602	**0.0000**	**0.0356**	0.7105	0.9824
N-acetyl-lysine	6.21	1.77	3.95	4.35	3.23	**0.0000**	**0.0013**	**0.0000**	**0.0000**	**0.0000**
Chorismic acid	41.45	3.56	29.65	36.33	1.17	**0.0000**	**0.0048**	**0.0000**	**0.0000**	0.7347
Homoserine	**0.52**	1.39	**0.66**	**0.48**	1.57	**0.0035**	0.1231	0.0557	**0.0012**	**0.0375**
Norvaline	5.58	9.70	5.11	6.07	2.14	**0.0000**	**0.0000**	**0.0000**	**0.0000**	**0.0001**

Nucleotide metabolism

Uracil	**0.50**	**0.24**	**0.32**	**0.49**	**0.69**	**0.0000**	**0.0000**	**0.0000**	**0.0000**	**0.0239**
Thymine	**0.64**	1.30	1.08	**0.90**	1.26	**0.0139**	0.1344	0.6438	0.5592	0.1915
Adenine	1.13	**0.85**	1.22	1.06	1.08	0.4083	0.3163	0.1949	0.6950	0.6238
Guanine	**0.30**	**0.22**	**0.37**	**0.33**	**0.34**	**0.0000**	**0.0000**	**0.0000**	**0.0000**	**0.0000**
Guanosine	**0.13**	**0.04**	**0.06**	**0.09**	**0.05**	**0.0000**	**0.0000**	**0.0000**	**0.0000**	**0.0000**
Adenosine	**0.03**	**0.00**	**0.01**	**0.10**	**0.06**	**0.0000**	**0.0000**	**0.0000**	**0.0000**	**0.0000**
2-Deoxyadenosine	1.69	**0.53**	**0.05**	5.05	95.44	0.8309	0.8020	0.2494	0.5070	**0.0439**
2'-Deoxyinosine 5'-monophosphate	5.66	1.73	3.47	4.50	1.25	**0.0000**	**0.0002**	**0.0000**	**0.0000**	0.1238
Beta-Alanine	4.09	36.26	14.76	9.10	13.19	**0.0012**	**0.0000**	**0.0000**	**0.0000**	**0.0000**
Xanthosine	**0.33**	**0.44**	**0.37**	**0.66**	**0.93**	**0.0000**	**0.0027**	**0.0004**	0.0845	0.7596

Other

Phytol	**0.25**	**0.58**	2.11	**0.05**	**0.20**	0.4969	0.7847	0.6870	0.2181	0.4750
Tocopherol	**0.18**	**0.27**	**0.53**	**0.71**	**0.19**	**0.0000**	**0.0000**	**0.0116**	0.1435	**0.0000**
Tocopherolacetate	1.11	**0.54**	**0.88**	**0.89**	3.39	0.7197	0.0514	0.6783	0.6996	**0.0001**
Nicotianamine	1.14	**0.41**	**0.85**	**0.66**	**0.62**	0.8029	0.1195	0.7629	0.4246	0.3990
Kaempferol	7.59	**0.75**	2.17	3.60	3.68	**0.0000**	0.1494	**0.0001**	**0.0000**	**0.0000**
Apigenin	2088.8	25.71	1284.4	1216.4	713.14	**0.0000**	**0.0000**	**0.0000**	**0.0000**	**0.0000**
Homogentisate	**0.71**	**0.88**	**0.87**	**0.73**	1.33	**0.0083**	0.2964	0.2840	**0.0140**	**0.0244**
Glucarate	**0.92**	4.19	3.36	1.97	**0.65**	0.7869	**0.0000**	**0.0003**	**0.0362**	0.2208

Ascorbic acid	**0.67**	8.75	5.44	2.05	**0.72**	0.0704	**0.0000**	**0.0000**	**0.0010**	0.1569
5-Hydroxy-tryptamine	10.36	4.43	8.69	6.34	2.22	**0.0000**	**0.0000**	**0.0000**	**0.0000**	**0.0000**
Pyroglutamic acid	3.67	**0.14**	**0.53**	2.43	1.96	**0.0001**	**0.0000**	0.0635	**0.0055**	**0.0390**
Gallic Acid	**0.65**	1.04	**0.86**	**0.58**	1.92	**0.0023**	0.7562	0.2822	**0.0002**	**0.0000**
Gallic acid ethyl ester	1.13	1.96	1.56	1.40	2.45	0.3605	**0.0000**	**0.0017**	**0.0150**	**0.0000**
2-Piperidinecarboxylic acid	5.92	**0.53**	1.84	2.96	2.83	**0.0000**	**0.0008**	**0.0005**	**0.0000**	**0.0000**
Phosphoric acid	**0.56**	**0.13**	**0.27**	**0.35**	**0.90**	**0.0010**	**0.0000**	**0.0000**	**0.0000**	0.5464

885

886

887 **Table 5.** Estimates of compound activity in four algal strains assayed using Nile red fluorescence to
888 measure neutral lipid accumulation.

		C.reinhardtii CC125	*C. vulgaris* UTEX395	*C. sorokiniana* UTEX1230	*Tetrachlorella alterns* UTEX2453
Structural Group	Compound	Nile Red fold change (NFC) ± SEM			
1	WD40844	9.83 ± 0.21	1.66 ± 0.24	2.42 ± 0.13	2.80 ± 0.20
1	WDTHQ130	6.46 ± 0.22	21.20 ± 3.10	6.17 ± 0.86	15.92 ± 0.70
1	WD40157	2.90 ± 0.40	9.04 ± 1.13	3.59 ± 0.32	4.46 ± 0.15
1	WD10784*	15.75 ± 3.27	6.51 ± 0.78	4.71 ± 0.95	11.33 ± 0.52
2	WD10738	13.65 ± 0.26	16.05 ± 1.87	4.79 ± 0.52	16.47 ± 0.84
2	WD10599	11.83 ± 0.25	11.86 ± 0.54	5.81 ± 0.83	17.32 ± 3.32
2	WD10461	14.57 ± 1.27	15.82 ± 2.47	4.78 ± 0.27	5.62 ± 0.17
2	WD10256	7.41 ± 1.00	13.80 ± 3.10	5.94 ± 0.61	24.49 ± 3.25
2	WD10264	10.01 ± 0.64	14.40 ± 1.18	5.48 ± 1.01	27.66 ± 1.66
3	WD30030	10.07 ± 0.84	16.60 ± 3.74	6.41 ± 1.07	19.05 ± 2.09
3	WD30999	10.09 ± 1.16	22.59 ± 2.66	7.15 ± 1.23	26.19 ± 0.82
4	WD10872	9.68 ± 1.42	11.53 ± 1.22	3.94 ± 0.84	6.62 ± 1.05
4	WD10615	10.12 ± 1.30	11.77 ± 0.41	4.80 ± 0.21	10.69 ± 1.35
5	WD20542	15.23 ± 1.85	13.51 ± 0.03	5.92 ± 0.87	10.30 ± 0.41
5	WD20067	10.61 ± 1.86	24.24 ± 1.19	5.40 ± 0.75	12.77 ± 1.07

889 Cultures (200 uL) were treated with 30 μM compound for 72 hr except for WD10784 (highlighted by asterisk)
890 where the concentration was 10 μM. Data is presented in NFC as mean of three experiments ± SEM. Additional
891 results for concentrations ranging from 0.625 to 50 μM is presented in supplemental information Table S2.
892

REFERENCES

Akula R, Giridhar P, Ravishankar GA (2011) Phytoserotonin. Plant Signaling & Behavior **6:** 800-809

Allen JW, DiRusso CC, Black PN (2015) Triacylglycerol synthesis during nitrogen stress involves the prokaryotic lipid synthesis pathway and acyl chain remodeling in the microalgae Coccomyxa subellipsoidea. Algal Research **10:** 110-120

Allen JW, DiRusso CC, Black PN (2017) Carbon and Acyl Chain Flux during Stress-induced Triglyceride Accumulation by Stable Isotopic Labeling of the Polar Microalga Coccomyxa subellipsoidea C169. J Biol Chem **292:** 361-374

Awai K, Xu C, Lu B, Benning C (2006) Lipid trafficking between the endoplasmic reticulum and the chloroplast. Biochemical Society transactions **34:** 395-398

Benning C (2008) A role for lipid trafficking in chloroplast biogenesis. Progress in lipid research **47:** 381-389

Bolling C, Fiehn O (2005) Metabolite profiling of Chlamydomonas reinhardtii under nutrient deprivation. Plant Physiology **139:** 1995-2005

Cakmak T, Angun P, Demiray YE, Ozkan AD, Elibol Z, Tekinay T (2012) Differential effects of nitrogen and sulfur deprivation on growth and biodiesel feedstock production of Chlamydomonas reinhardtii. Biotechnology and bioengineering **109:** 1947-1957

Chapman SP, Paget CM, Johnson GN, Schwartz JM (2015) Flux balance analysis reveals acetate metabolism modulates cyclic electron flow and alternative glycolytic pathways in Chlamydomonas reinhardtii. Front Plant Sci **6:** 474

Chen W, Zhang CW, Song LR, Sommerfeld M, Hu Q (2009) A high throughput Nile red method for quantitative measurement of neutral lipids in microalgae. J Microbiol Meth **77:** 41-47

Choi YE, Rhee JK, Kim HS, Ahn JW, Hwang H, Yang JW (2015) Chemical Genetics Approach Reveals Importance of cAMP and MAP Kinase Signaling to Lipid and Carotenoid Biosynthesis in Microalgae. J Microbiol Biotechnol **25:** 637-647

Franz AK, Danielewicz MA, Wong DM, Anderson LA, Boothe JR (2013) Phenotypic screening with oleaginous microalgae reveals modulators of lipid productivity. ACS Chem Biol **8:** 1053-1062

Goncalves EC, Johnson JV, Rathinasabapathi B (2013) Conversion of membrane lipid acyl groups to triacylglycerol and formation of lipid bodies upon nitrogen starvation in biofuel green algae Chlorella UTEX29. Planta **238:** 895-906

Greenspan P, Mayer EP, Fowler SD (1985) Nile red - a selective fluorescent stain for intracellular lipid droplets. J Cell Biol **100:** 965-973

Guarnieri MT, Nag A, Smolinski SL, Darzins A, Seibert M, Pienkos PT (2011) Examination of Triacylglycerol Biosynthetic Pathways via De Novo Transcriptomic and Proteomic Analyses in an Unsequenced Microalga. PloS one **6:** e25851

Guschina IA, Harwood JL (2009) Algal Lipids and Effect of the Environment on their Biochemistry. Springer New York

Hall LH, Kier LB (1995) Electrotopological state indices for atom types: a novel combination of electronic, topological, and valence state information. Journal of Chemical Information and Computer Sciences **35:** 1039-1045

Harris EH (2009) The Chlamydomonas sourcebook: introduction to Chlamydomonas and its laboratory use, Vol 1. Academic Press

Hu Q, Sommerfeld M, Jarvis E, Ghirardi M, Posewitz M, Seibert M, Darzins A (2008) Microalgal triacylglycerols as feedstocks for biofuel production: perspectives and advances. The Plant journal : for cell and molecular biology **54:** 621-639

Jones CS, Mayfield SP (2012) Algae biofuels: versatility for the future of bioenergy. Current opinion in biotechnology **23:** 346-351

Kim H, Jang S, Kim S, Yamaoka Y, Hong D, Song WY, Nishida I, Li-Beisson Y, Lee Y (2015) The small molecule fenpropimorph rapidly converts chloroplast membrane lipids to triacylglycerols in Chlamydomonas reinhardtii. Front Microbiol **6:** 54

Li J, Niu X, Pei G, Sui X, Zhang X, Chen L, Zhang W (2015) Identification and metabolomic analysis of chemical modulators for lipid accumulation in Crypthecodinium cohnii. Bioresour Technol **191:** 362-368

Lichtenthaler HK, Wellburn AR (1983) Determinations of total carotenoids and chlorophylls a and b of leaf extracts in different solvents. Biochemical Society Transactions **11:** 591-592

Lipinski CA, Lombardo F, Dominy BW, Feeney PJ (1997) Experimental and computational approaches to estimate solubility and permeability in drug discovery and development settings. Advanced Drug Delivery Reviews **23:** 3-25

Longworth J, Noirel J, Pandhal J, Wright PC, Vaidyanathan S (2012) HILIC-and SCX-based quantitative proteomics of Chlamydomonas reinhardtii during nitrogen starvation induced lipid and carbohydrate accumulation. Journal of proteome research **11:** 5959-5971

Mallick N, Mandal S, Singh AK, Bishai M, Dash A (2012) Green microalga Chlorella vulgaris as a potential feedstock for biodiesel. Journal of Chemical Technology & Biotechnology **87:** 137-145

McCourt P, Desveaux D (2010) Plant chemical genetics. New Phytol **185:** 15-26

Morita E, Kumon Y Fau - Nakahara T, Nakahara T Fau - Kagiwada S, Kagiwada S Fau - Noguchi T, Noguchi T (2006) Docosahexaenoic acid production and lipid-body formation in Schizochytrium limacinum SR21. Marine Biotechnology **8:** 319-327

960 **Msanne J, Xu D, Konda AR, Casas-Mollano JA, Awada T, Cahoon EB, Cerutti H** (2012) Metabolic and gene
961 expression changes triggered by nitrogen deprivation in the photoautotrophically grown microalgae
962 Chlamydornonas reinhardtii and Coccomyxa sp C-169. Phytochemistry **75:** 50-59
963 **Rosenberg JN, Kobayashi N, Barnes A, Noel EA, Betenbaugh MJ, Oyler GA** (2014) Comparative analyses of
964 three Chlorella species in response to light and sugar reveal distinctive lipid accumulation patterns in the
965 Microalga C. sorokiniana. PLoS One **9:** e92460
966 **Sak K** (2014) Cytotoxicity of dietary flavonoids on different human cancer types. Pharmacogn Rev **8:** 122-146
967 **Schaffer JE** (2003) Lipotoxicity: when tissues overeat. Current opinion in lipidology **14:** 281
968 **Scranton MA, Ostrand JT, Fields FJ, Mayfield SP** (2015) Chlamydomonas as a model for biofuels and bio-
969 products production. Plant J **82:** 523-531
970 **Song X, Zang X Fau - Zhang X, Zhang X** (2015) Production of high docosahexaenoic acid by Schizochytrium sp.
971 using low-cost raw materials from food industry J Oleo Sci **64:** 197-204
972 **Specht EA, Nour-Eldin HH, Hoang KT, Mayfield SP** (2015) An improved ARS2-derived nuclear reporter enhances
973 the efficiency and ease of genetic engineering in Chlamydomonas. Biotechnol J **10:** 473-479
974 **Sung B, Chung HY, Kim ND** (2016) Role of Apigenin in Cancer Prevention via the Induction of Apoptosis and
975 Autophagy. J Cancer Prev **21:** 216-226
976 **Unger RH, Scherer PE** (2010) Gluttony, sloth and the metabolic syndrome: a roadmap to lipotoxicity. Trends
977 Endocrinol Metab **21:** 345-352
978 **Urzica EI, Vieler A, Hong-Hermesdorf A, Page MD, Casero D, Gallaher SD, Kropat J, Pellegrini M, Benning C,**
979 **Merchant SS** (2013) Remodeling of Membrane Lipids in Iron-starved Chlamydomonas. Journal of Biological
980 Chemistry **288:** 30246-30258
981 **Wallace I, Bader G, Giaever G, Nislow C** (2011) Displaying Chemical Information on a Biological Network Using
982 Cytoscape. *In* G Cagney, A Emili, eds, Network Biology, Vol 781. Humana Press, pp 363-376
983 **Wan M-X, Wang R-M, Xia J-L, Rosenberg JN, Nie Z-Y, Kobayashi N, Oyler GA, Betenbaugh MJ** (2012)
984 Physiological evaluation of a new Chlorella sorokiniana isolate for its biomass production and lipid
985 accumulation in photoautotrophic and heterotrophic cultures. Biotechnology and Bioengineering **109:** 1958-
986 1964
987 **Wang D, Lu Y, Huang H, Xu J** (2012) Establishing oleaginous microalgae research models for consolidated
988 bioprocessing of solar energy. Advances in biochemical engineering/biotechnology **128:** 69-84
989 **Wase N, Black PN, Stanley BA, DiRusso CC** (2014) Integrated quantitative analysis of nitrogen stress response in
990 Chlamydomonas reinhardtii using metabolite and protein profiling. J Proteome Res **13:** 1373-1396
991 **Wase N, Tu BQ, Black PN, DiRusso CC** (2015) Phenotypic screening identifies Brefeldin A/Ascotoxin as an inducer
992 of lipid storage in the algae *Chlamydomonas reinhardtii*. Algal Research-Biomass Biofuels and Bioproducts
993 **11:** 74-84

994 **Weng CJ, Yen GC** (2012) Flavonoids, a ubiquitous dietary phenolic subclass, exert extensive in vitro anti-invasive
995 and in vivo anti-metastatic activities. Cancer Metastasis Rev **31:** 323-351
996 **Wetzel S, Klein K, Renner S, Rauh D, Oprea TI, Mutzel P, Waldmann H** (2009) Interactive exploration of
997 chemical space with Scaffold Hunter. Nat Chem Biol **5:** 581-583
998 **Yeung N, Cline MS, Kuchinsky A, Smoot ME, Bader GD** (2002) Exploring Biological Networks with Cytoscape
999 Software. *In* Current Protocols in Bioinformatics. John Wiley & Sons, Inc.
1000 **Zhang JH, Chung TD, Oldenburg KR** (1999) A Simple Statistical Parameter for Use in Evaluation and Validation
1001 of High Throughput Screening Assays. J Biomol Screen **4:** 67-73
1002
1003
1004
1005

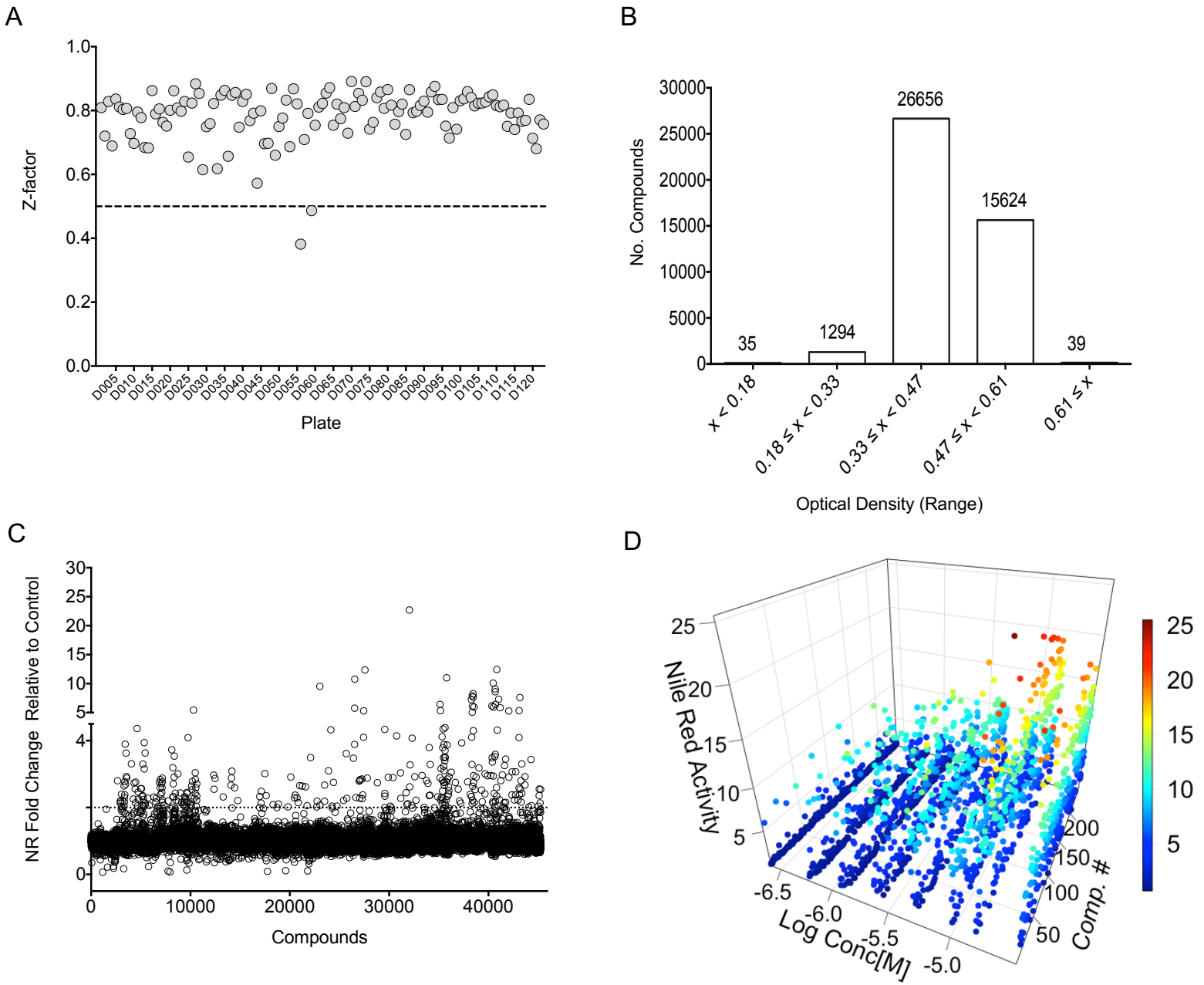

Figure 1. Summary of results of high throughput screening. A, Z-factor calculation for each of 124 plates totaling 43,736 compounds. The average Z' value was 0.78 ± 0.08 with a coefficient of variation (CV) of 14.4%. B, Growth measured as OD_{600} in the presence of compound after 72h. The average of the N+ control cells was 0.41 ± 0.04. C, Lipid accumulation measured as relative fluorescence after Nile Red (NR) staining of cells treated with compound relative to cells treated with vehicle (DMSO). D, Confirmation of hits and dose response. Data for 243 compounds are shown fitting the concentration response curve (from 0.25 μM to 30 μM) to lipid accumulation. The scale bar represents the relative fold change of treatment to control (y-axis).

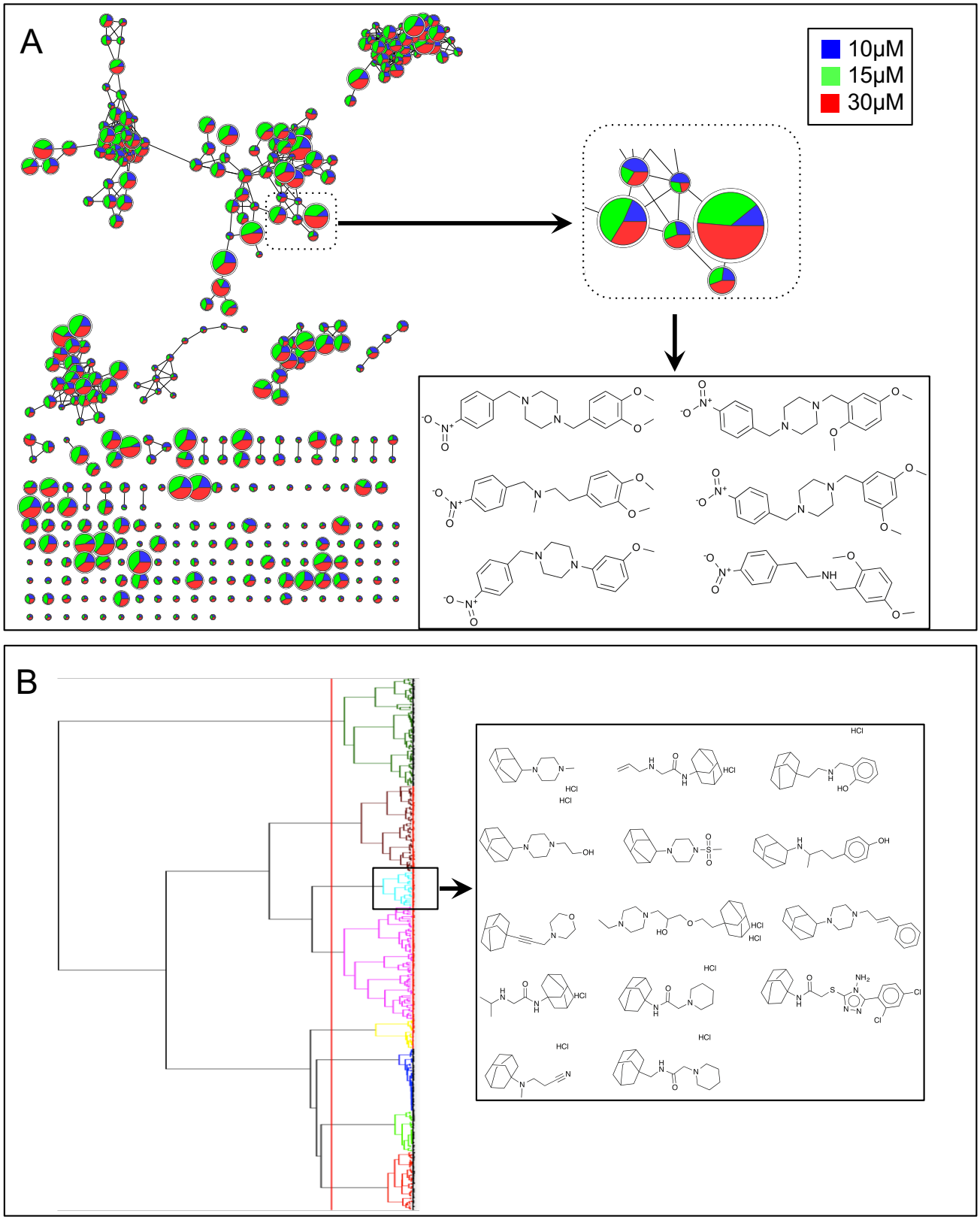

Figure 2. Structural comparisons of hits from the primary screen. A, Network view of lipid accumulating small molecules. Compounds identified in the primary screen and verified using an 8-point dose response curve were clustered according to their Tanimoto similarity score. Each node represents a unique small molecule. Edges represent the structural similarities at a Tanimoto score cuttoff of 0.70. Data for the relevant compound at 30 μM (red), 15 μM (green) and 10 μM (blue) are mapped in a pie chart. The node size represents the fold change of each chemical (30 μM). A portion of the network is magnified to show clustered compounds having structural similarities. B, Clustering analysis of active compounds using Ward's linkage method. Distance was calculated based on Tanimoto coefficient and Estate bit fingerprints were used for similarity calculations. One of the clusters was highlighted showing the admantane moiety. Note, some of the compounds are presented as salts of HCl. 2 HCl molecules indicate chiral diamantoiners.

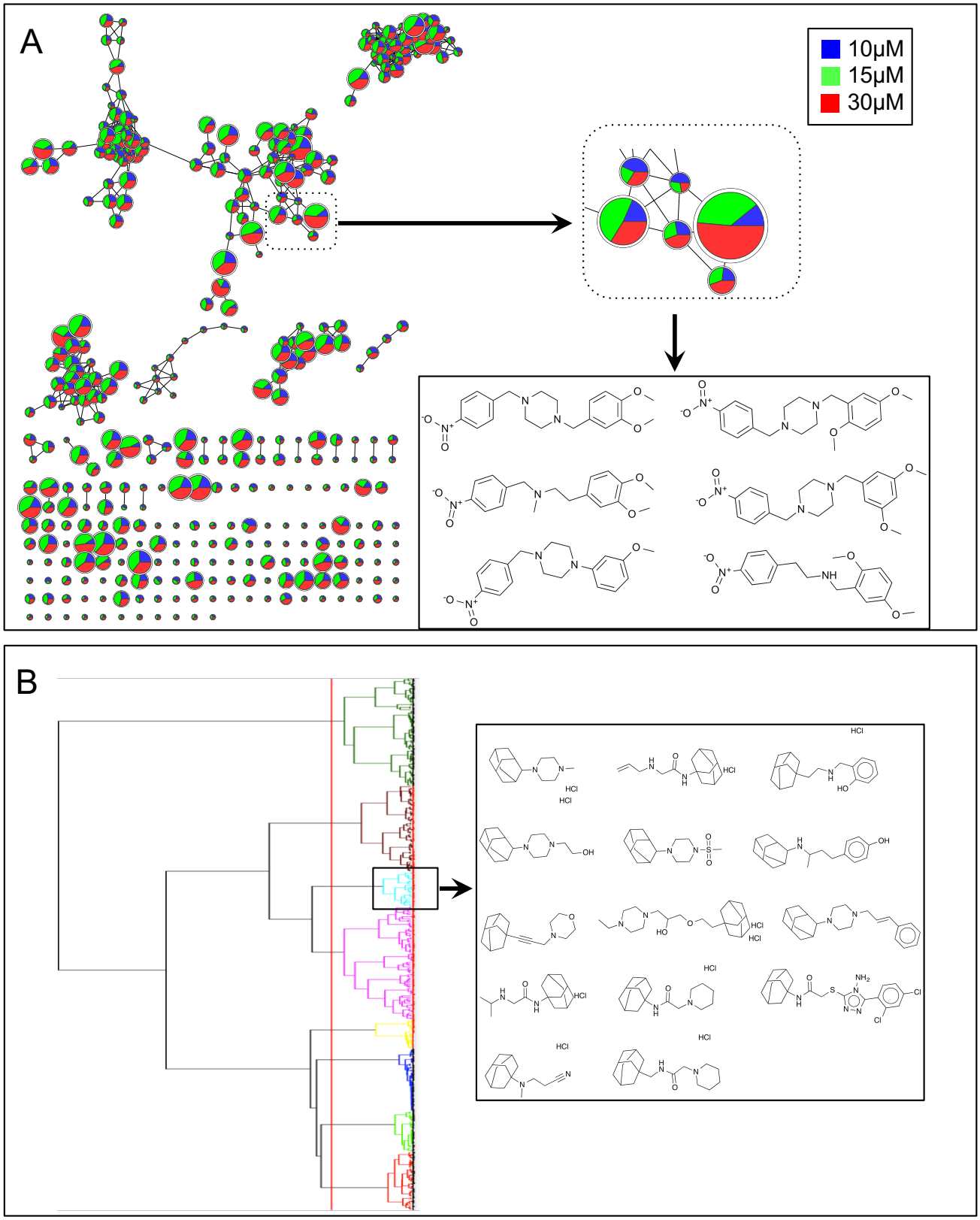

Figure 2. Structural comparisons of hits from the primary screen. A, Network view of lipid accumulating small molecules. Compounds identified in the primary screen and verified using an 8-point dose response curve were clustered according to their Tanimoto similarity score. Each node represents a unique small molecule. Edges represent the structural similarities at a Tanimoto score cuttoff of 0.70. Data for the relevant compound at 30 μM (red), 15 μM (green) and 10 μM (blue) are mapped in a pie chart. The node size represents the fold change of each chemical (30 μM). A portion of the network is magnified to show clustered compounds having structural similarities. B, Clustering analysis of active compounds using Ward's linkage method. Distance was calculated based on Tanimoto coefficient and Estate bit fingerprints were used for similarity calculations. One of the clusters was highlighted showing the admantane moiety. Note, some of the compounds are presented as salts of HCl. 2 HCl molecules indicate chiral diamantoiners.

Control

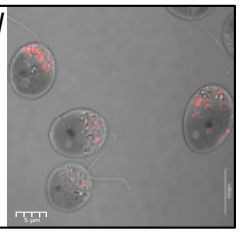

Group 1

WD408844

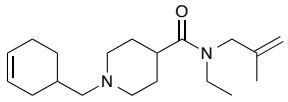

1-(cyclohex-3-en-1-ylmethyl)-*N*-ethyl-*N*-(2-methylallyl)piperidine-4-carboxamide

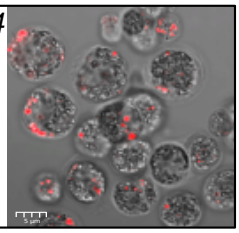

WD40157

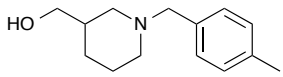

(1-(4-methylbenzyl)piperidin-3-yl)methanol

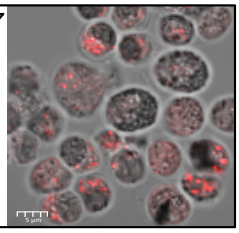

WDTHQ130

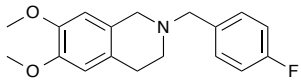

2-(4-fluorobenzyl)-6,7-dimethoxy-1,2,3,4-tetrahydroisoquinoline

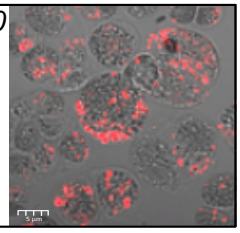

WD10784

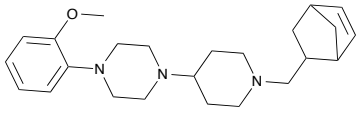

1-(1-(bicyclo[2.2.1]hept-5-en-2-ylmethyl) piperidin-4-yl)-4-(2-methoxyphenyl) piperazine

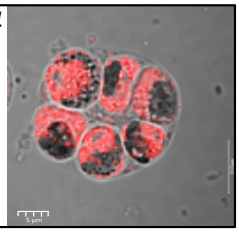

Group 2

WD10738

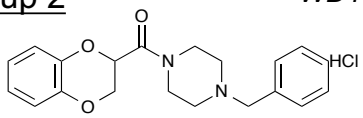

(4-benzylpiperazin-1-yl)(2,3-dihydrobenzo[*b*] 1,4]dioxin-2-yl) methanone hydrochloride

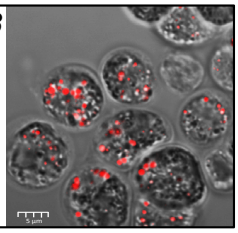

WD10461

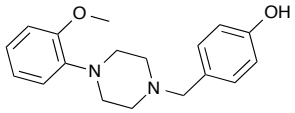

4-((4-(2-methoxyphenyl)piperazin-1-yl)methyl)phenol

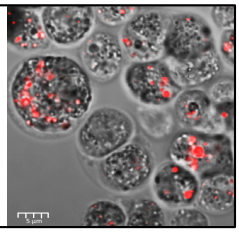

WD10264

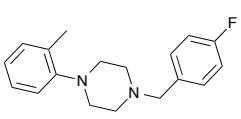

1-(4-fluorobenzyl)-4-(*o*-tolyl)piperazine

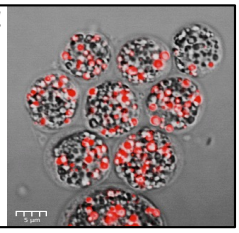

Group 2 (cont.)

WD10599

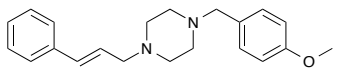

1-cinnamyl-4-(4-methoxybenzyl)piperazine

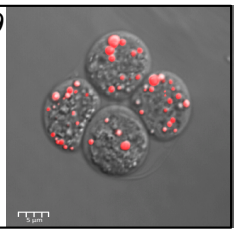

WD10256

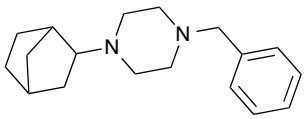

1-benzyl-4-(bicyclo[2.2.1]heptan-2-yl)piperazine

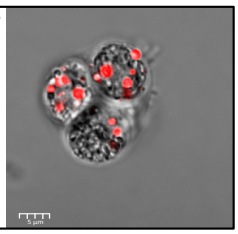

Group 3

WD30030

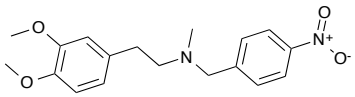

2-(3,4-dimethoxyphenyl)-*N*-methyl-*N*- (4-nitrobenzyl)ethan-1-amine

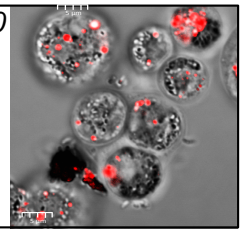

WD30999

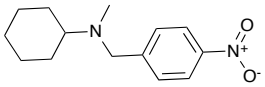

N-methyl-*N*-(4-nitrobenzyl) cyclohexanamine

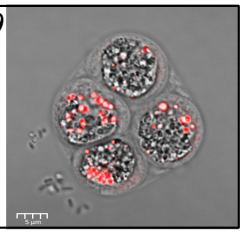

Group 4

WD10872

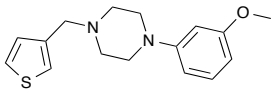

1-(3-methoxyphenyl)-4-(thiophen-3-ylmethyl) piperazine

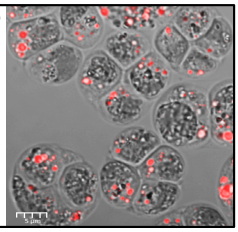

WD10615

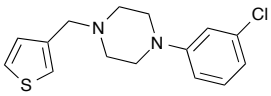

1-(3-chlorophenyl)-4-(thiophen-3-yl methyl) piperazine

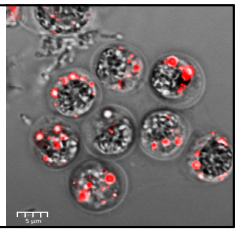

Group 5

WD20542

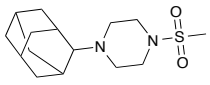

1-(adamantan-2-yl)-4-(methylsulfonyl) piperazine

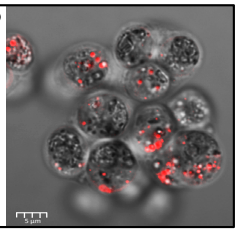

WD20067

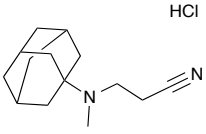

3-(adamantan-1-yl(methyl)amino) propanenitrile hydrochloride

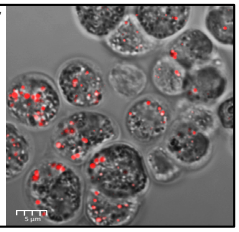

Figure 3. Lipid body accumulation in *C. reinhardtii* induced by diverse compounds.

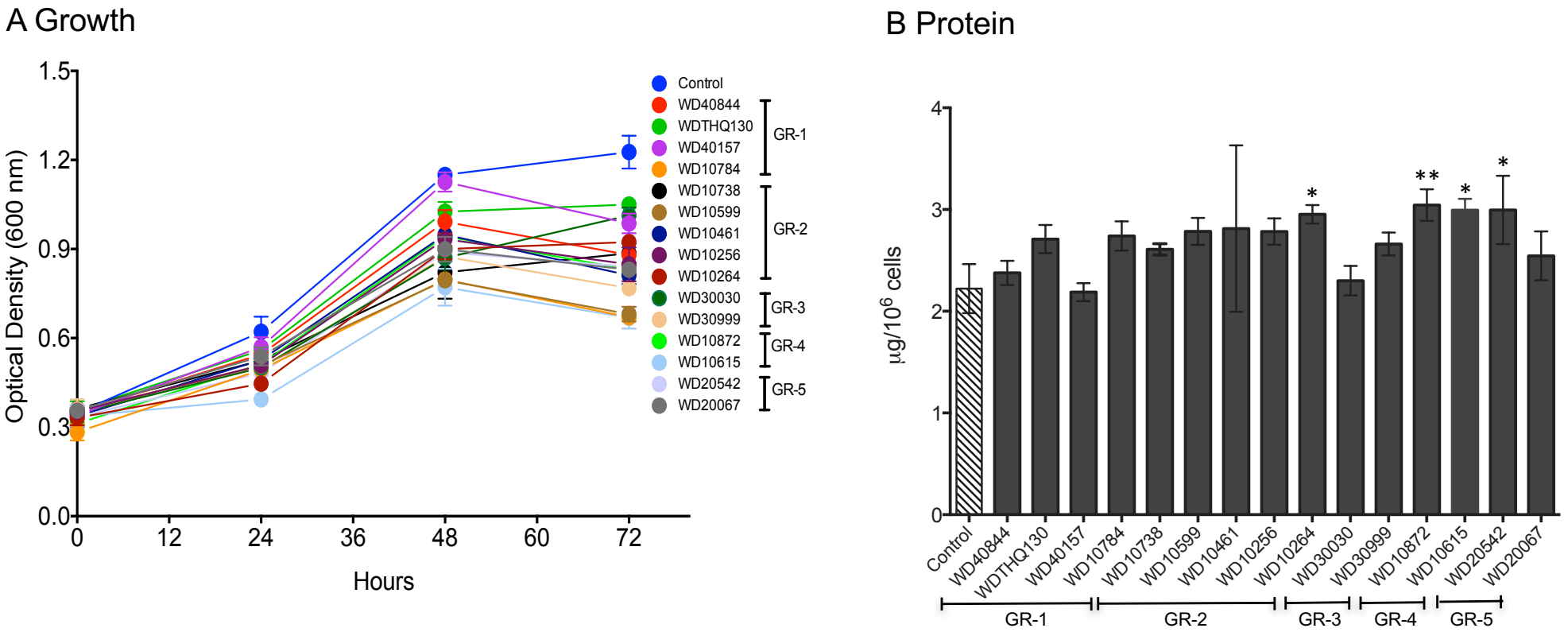

Figure 4. Growth of cells and accumulation of protein during compound treatment. A, Cells were treated with 30 µM of the specified compounds as indicated and OD_{600} was monitored over 72h (n=3; ± SD); B, after harvesting, total protein levels were measured per 10^6 cells. Bar height indicates the mean of 3 biological replicates (n=3 ± SD). Significance of difference in the levels of total protein was assessed using ANOVA to compare the treated samples to controls (* p<0.05; **, p< 0.01; ***, p< 0.001).

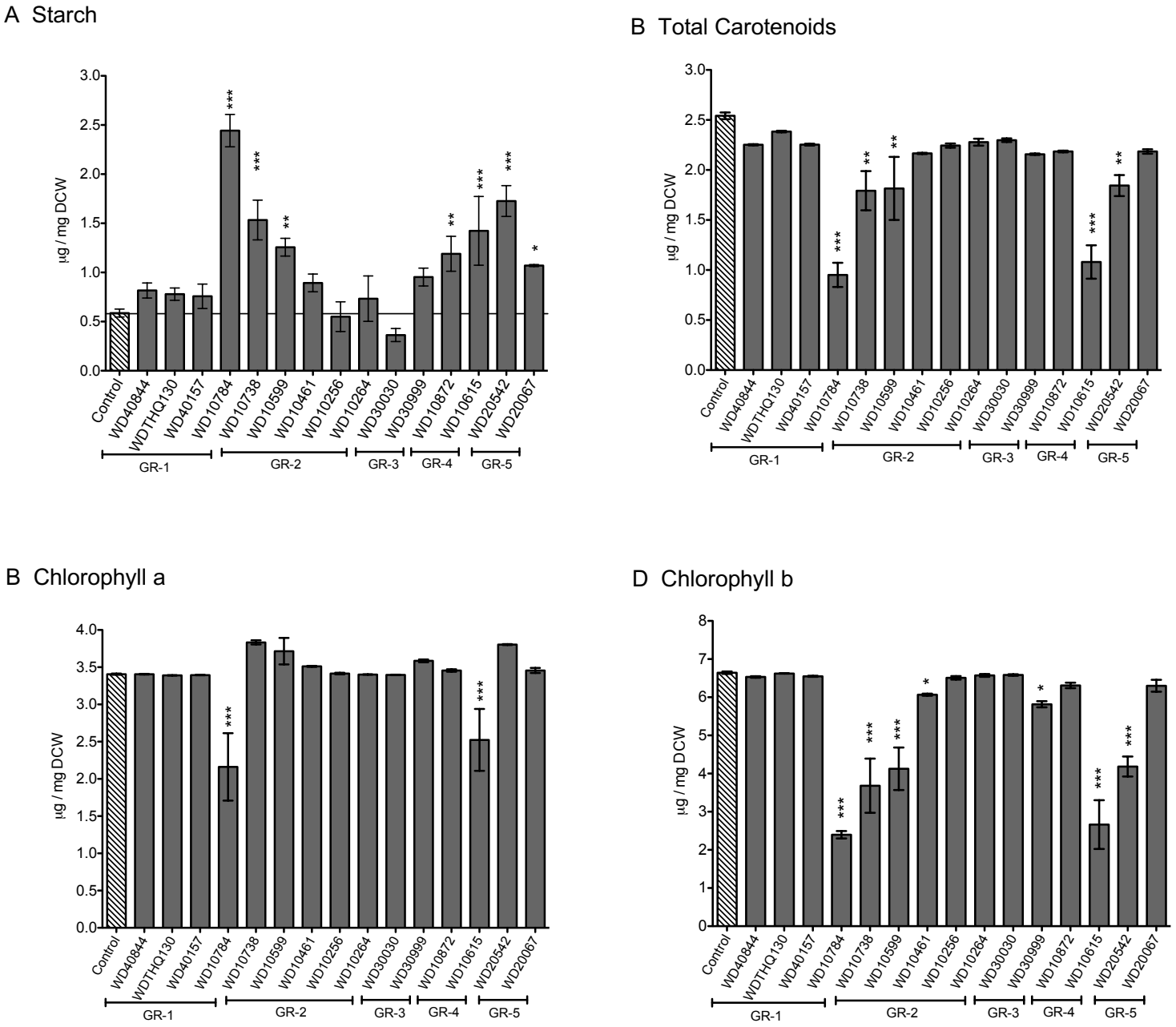

Figure 5. Assessment of cellular macromolecule accumulation after treatment with selected compounds for 72h. A, Total starch; B, total carotenoids; C, chlorophyll a; and D, chlorophyll b. Bar height indicates the mean of 3 independent experiments (± SD). The controls were values obtained for cultures treated with the vehicle DMSO. ANOVA (JMP v11) was applied to determine the significance of differences in the levels of total protein as compared to untreated control cells (N+) (* $p<0.05$; ** $p<0.01$; *** $p<0.001$).

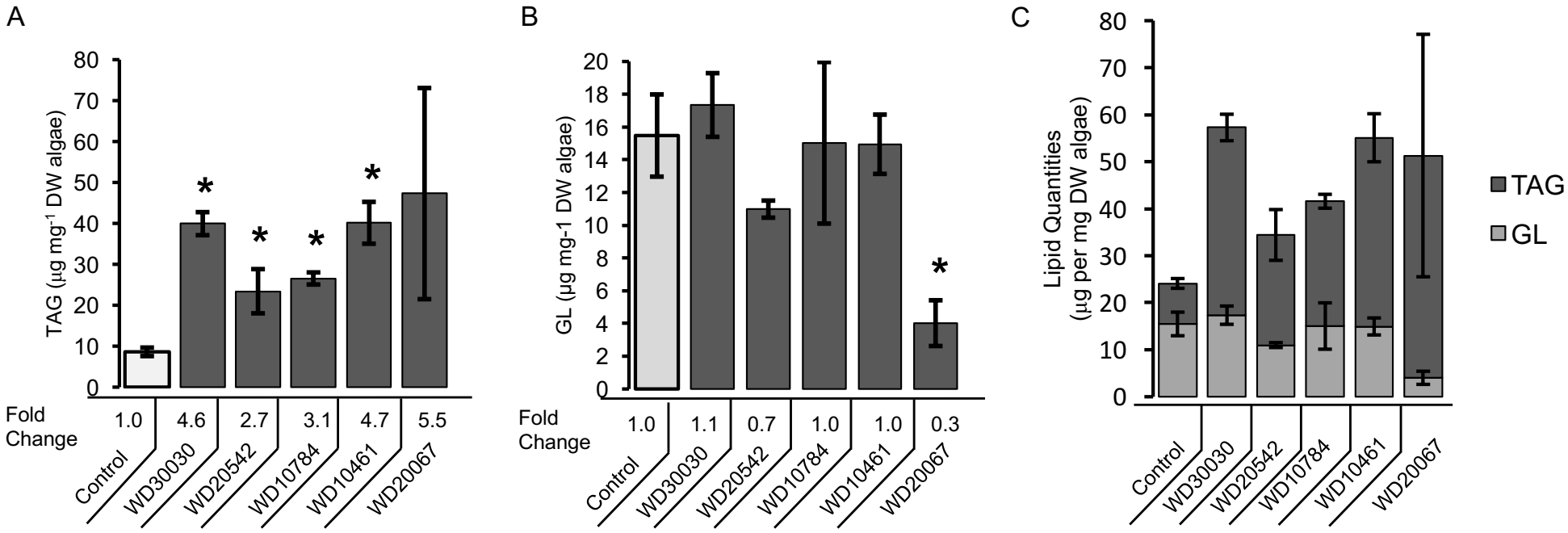

Figure 6. Identification and quantification of complex lipids by LC-MS/MS. Total A, triglycerides (TAG) and B, galactolipids (GL) are presented by comparison with control levels. Height of the bar is the mean and error bars give the S.E.M. C, Relative quantities of TAG and GL as indicated.

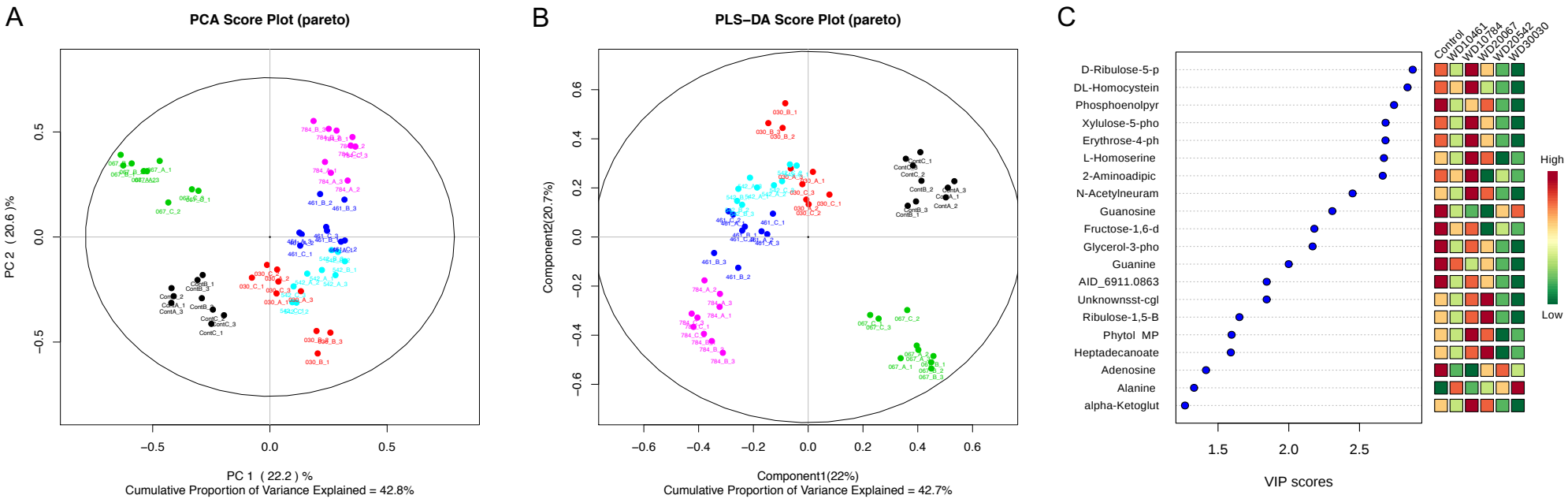

Figure 7. Univariate and multivariate analysis of the GC-MS metabolites. A, PCA of primary metabolites/features of compound treated and untreated control samples. Control (black), WD30030 (red), compound WD20542 (cyan), compound WD10461 (blue), compound WD20067 (green) and compound WD10784 (pink). B, Partial Least Square-Discriminate Analysis (PLS-DA) of the data for better separation of the samples to identify features that are responsible for differentiation in the treatment. C, Top 20 metabolites with significantly different abundance between compound treatments based on the VIP projection deduced using Metaboanalyst web tool (http://www.metaboanalyst.ca).

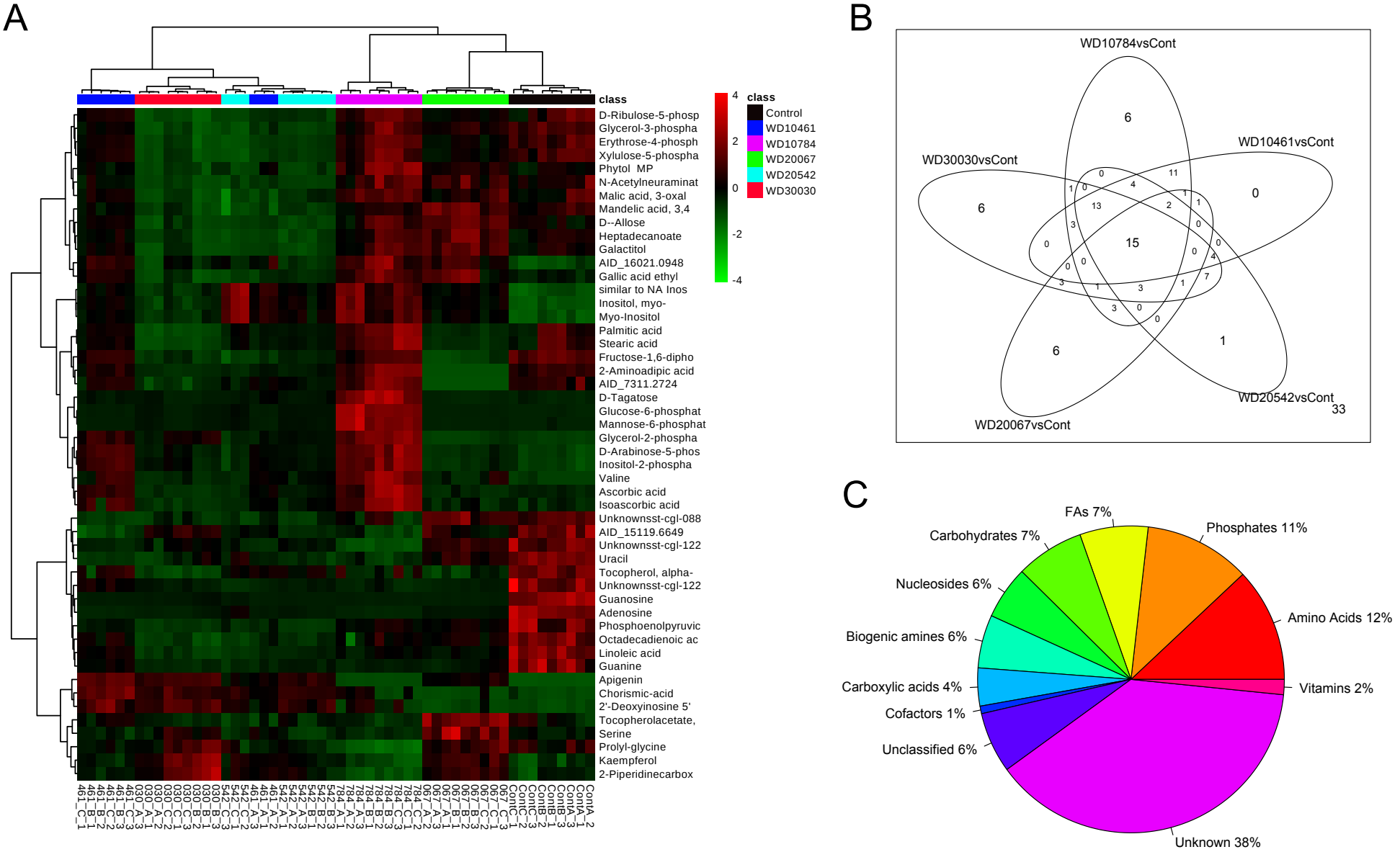

Figure 8. Summary of metabolite profiling experiments. A, Heatmap showing the metabolite abundance profiles of compound treated versus control cells. The expression levels of the top 50 metabolites selected after applying ANOVA $p < 0.05$ are illustrated. B, Venn diagram showing the unique and common differentially changed features/metabolites in different compound treated metabolomes. The numbers of peaks that were not significantly changed (33) are shown at the bottom right. C, Metabolite peaks generated after peak picking and deconvulation, were identified using the MassBank and GOLM metabolome libraries. For each identified feature, a KEGG compound code was assigned as per KEGG brite and classified according to their biological role.

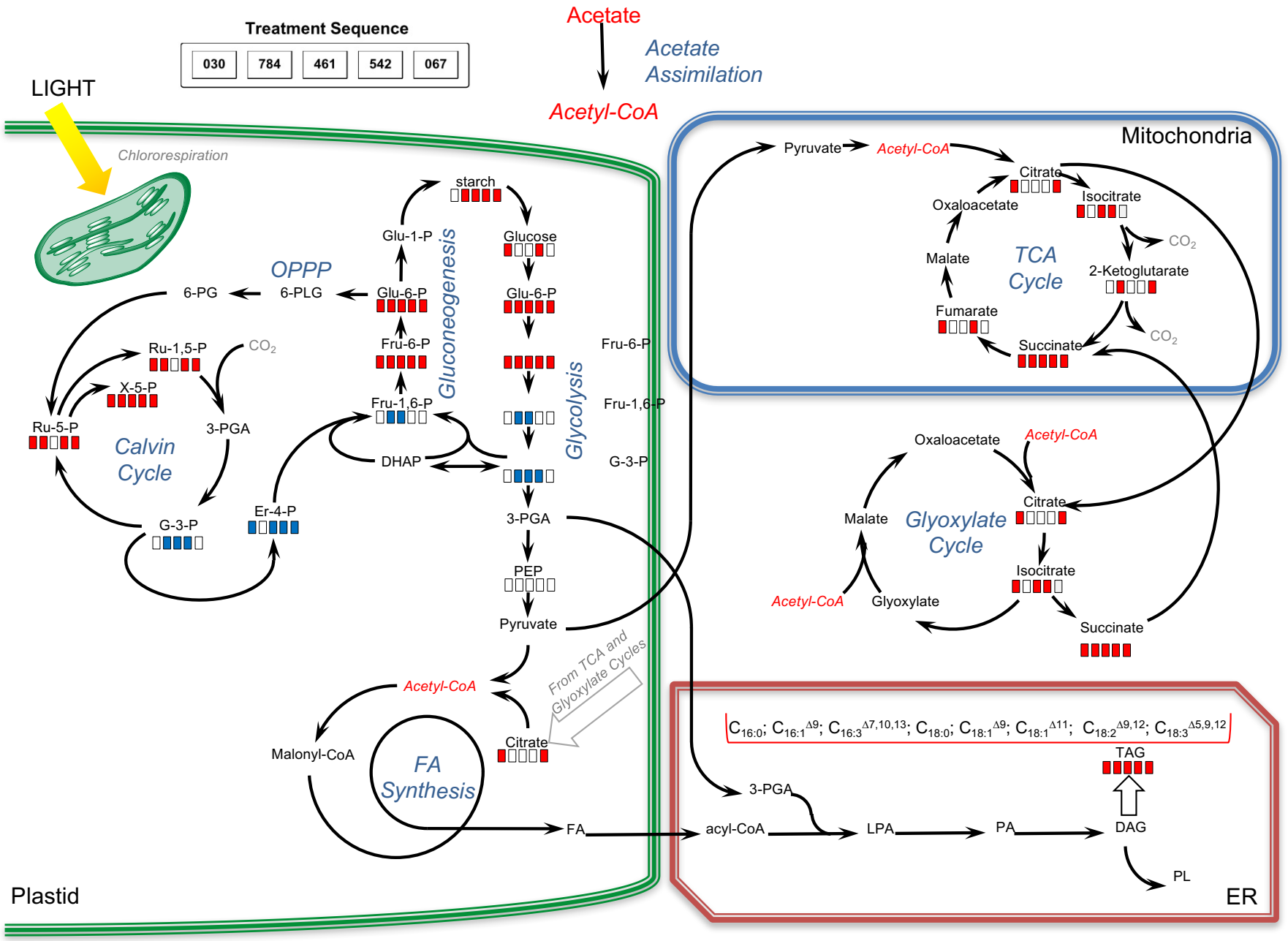

Figure 9. Pathway map representing the impact of various compounds on carbon metabolism. Red bar indicates significantly increased levels of metabolites in compound treated samples relative to controls; blue indicates significantly decreased levels of metabolites in compound treated samples relative to controls; and white indicates no significant difference between treated and control samples. For quantitation of changes see Table 4 and Supplemental Information 1 Tables S4A and S4B.

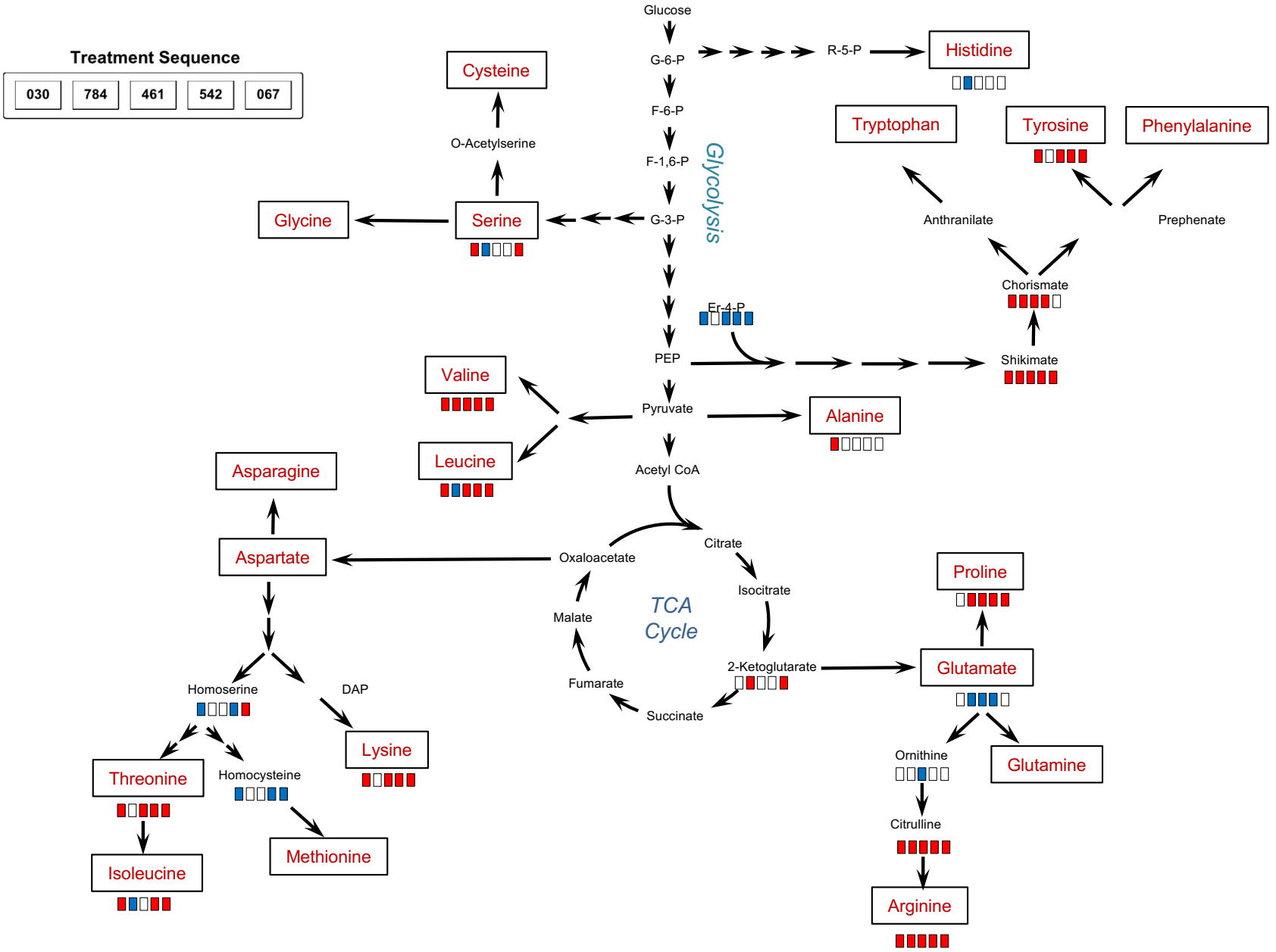

Figure 10. Pathway map illustrating the impact of various compounds on amino acid biosynthesis. Red bar indicates significantly increased levels of metabolites in compound treated samples relative to controls; blue indicates significantly decreased levels; and white indicates no significant difference between treated and control samples. For quantitation of changes see Table 4.

Parsed Citations

Akula R, Giridhar P, Ravishankar GA (2011) Phytoserotonin. Plant Signaling & Behavior 6: 800-809
Pubmed: Author and Title
CrossRef: Author and Title
Google Scholar: Author Only Title Only Author and Title

Allen JW, DiRusso CC, Black PN (2015) Triacylglycerol synthesis during nitrogen stress involves the prokaryotic lipid synthesis pathway and acyl chain remodeling in the microalgae Coccomyxa subellipsoidea. Algal Research 10: 110-120
Pubmed: Author and Title
CrossRef: Author and Title
Google Scholar: Author Only Title Only Author and Title

Allen JW, DiRusso CC, Black PN (2017) Carbon and Acyl Chain Flux during Stress-induced Triglyceride Accumulation by Stable Isotopic Labeling of the Polar Microalga Coccomyxa subellipsoidea C169. J Biol Chem 292: 361-374
Pubmed: Author and Title
CrossRef: Author and Title
Google Scholar: Author Only Title Only Author and Title

Awai K, Xu C, Lu B, Benning C (2006) Lipid trafficking between the endoplasmic reticulum and the chloroplast. Biochemical Society transactions 34: 395-398
Pubmed: Author and Title
CrossRef: Author and Title
Google Scholar: Author Only Title Only Author and Title

Benning C (2008) A role for lipid trafficking in chloroplast biogenesis. Progress in lipid research 47: 381-389
Pubmed: Author and Title
CrossRef: Author and Title
Google Scholar: Author Only Title Only Author and Title

Bolling C, Fiehn O (2005) Metabolite profiling of Chlamydomonas reinhardtii under nutrient deprivation. Plant Physiology 139: 1995-2005
Pubmed: Author and Title
CrossRef: Author and Title
Google Scholar: Author Only Title Only Author and Title

Cakmak T, Angun P, Demiray YE, Ozkan AD, Elibol Z, Tekinay T (2012) Differential effects of nitrogen and sulfur deprivation on growth and biodiesel feedstock production of Chlamydomonas reinhardtii. Biotechnology and bioengineering 109: 1947-1957
Pubmed: Author and Title
CrossRef: Author and Title
Google Scholar: Author Only Title Only Author and Title

Chapman SP, Paget CM, Johnson GN, Schwartz JM (2015) Flux balance analysis reveals acetate metabolism modulates cyclic electron flow and alternative glycolytic pathways in Chlamydomonas reinhardtii. Front Plant Sci 6: 474
Pubmed: Author and Title
CrossRef: Author and Title
Google Scholar: Author Only Title Only Author and Title

Chen W, Zhang CW, Song LR, Sommerfeld M, Hu Q (2009) A high throughput Nile red method for quantitative measurement of neutral lipids in microalgae. J Microbiol Meth 77: 41-47
Pubmed: Author and Title
CrossRef: Author and Title
Google Scholar: Author Only Title Only Author and Title

Choi YE, Rhee JK, Kim HS, Ahn JW, Hwang H, Yang JW (2015) Chemical Genetics Approach Reveals Importance of cAMP and MAP Kinase Signaling to Lipid and Carotenoid Biosynthesis in Microalgae. J Microbiol Biotechnol 25: 637-647
Pubmed: Author and Title
CrossRef: Author and Title
Google Scholar: Author Only Title Only Author and Title

Franz AK, Danielewicz MA, Wong DM, Anderson LA, Boothe JR (2013) Phenotypic screening with oleaginous microalgae reveals modulators of lipid productivity. ACS Chem Biol 8: 1053-1062
Pubmed: Author and Title
CrossRef: Author and Title
Google Scholar: Author Only Title Only Author and Title

Goncalves EC, Johnson JV, Rathinasabapathi B (2013) Conversion of membrane lipid acyl groups to triacylglycerol and formation of lipid bodies upon nitrogen starvation in biofuel green algae Chlorella UTEX29. Planta 238: 895-906
Pubmed: Author and Title
CrossRef: Author and Title
Google Scholar: Author Only Title Only Author and Title

Greenspan P, Mayer EP, Fowler SD (1985) Nile red - a selective fluorescent stain for intracellular lipid droplets. J Cell Biol 100: 965-973
Pubmed: Author and Title
CrossRef: Author and Title
Google Scholar: Author Only Title Only Author and Title

Guarnieri MT, Nag A, Smolinski SL, Darzins A, Seibert M, Pienkos PT (2011) Examination of Triacylglycerol Biosynthetic Pathways via De Novo Transcriptomic and Proteomic Analyses in an Unsequenced Microalga. PloS one 6: e25851

Pubmed: Author and Title
CrossRef: Author and Title
Google Scholar: Author Only Title Only Author and Title

Guschina IA, Harwood JL (2009) Algal Lipids and Effect of the Environment on their Biochemistry. Springer New York
Pubmed: Author and Title
CrossRef: Author and Title
Google Scholar: Author Only Title Only Author and Title

Hall LH, Kier LB (1995) Electrotopological state indices for atom types: a novel combination of electronic, topological, and valence state information. Journal of Chemical Information and Computer Sciences 35: 1039-1045
Pubmed: Author and Title
CrossRef: Author and Title
Google Scholar: Author Only Title Only Author and Title

Harris EH (2009) The Chlamydomonas sourcebook: introduction to Chlamydomonas and its laboratory use, Vol 1. Academic Press
Pubmed: Author and Title
CrossRef: Author and Title
Google Scholar: Author Only Title Only Author and Title

Hu Q, Sommerfeld M, Jarvis E, Ghirardi M, Posewitz M, Seibert M, Darzins A (2008) Microalgal triacylglycerols as feedstocks for biofuel production: perspectives and advances. The Plant journal : for cell and molecular biology 54: 621-639
Pubmed: Author and Title
CrossRef: Author and Title
Google Scholar: Author Only Title Only Author and Title

Jones CS, Mayfield SP (2012) Algae biofuels: versatility for the future of bioenergy. Current opinion in biotechnology 23: 346-351
Pubmed: Author and Title
CrossRef: Author and Title
Google Scholar: Author Only Title Only Author and Title

Kim H, Jang S, Kim S, Yamaoka Y, Hong D, Song WY, Nishida I, Li-Beisson Y, Lee Y (2015) The small molecule fenpropimorph rapidly converts chloroplast membrane lipids to triacylglycerols in Chlamydomonas reinhardtii. Front Microbiol 6: 54
Pubmed: Author and Title
CrossRef: Author and Title
Google Scholar: Author Only Title Only Author and Title

Li J, Niu X, Pei G, Sui X, Zhang X, Chen L, Zhang W (2015) Identification and metabolomic analysis of chemical modulators for lipid accumulation in Crypthecodinium cohnii. Bioresour Technol 191: 362-368
Pubmed: Author and Title
CrossRef: Author and Title
Google Scholar: Author Only Title Only Author and Title

Lichtenthaler HK, Wellburn AR (1983) Determinations of total carotenoids and chlorophylls a and b of leaf extracts in different solvents. Biochemical Society Transactions 11: 591-592
Pubmed: Author and Title
CrossRef: Author and Title
Google Scholar: Author Only Title Only Author and Title

Lipinski CA, Lombardo F, Dominy BW, Feeney PJ (1997) Experimental and computational approaches to estimate solubility and permeability in drug discovery and development settings. Advanced Drug Delivery Reviews 23: 3-25
Pubmed: Author and Title
CrossRef: Author and Title
Google Scholar: Author Only Title Only Author and Title

Longworth J, Noirel J, Pandhal J, Wright PC, Vaidyanathan S (2012) HILIC-and SCX-based quantitative proteomics of Chlamydomonas reinhardtii during nitrogen starvation induced lipid and carbohydrate accumulation. Journal of proteome research 11: 5959-5971
Pubmed: Author and Title
CrossRef: Author and Title
Google Scholar: Author Only Title Only Author and Title

Mallick N, Mandal S, Singh AK, Bishai M, Dash A (2012) Green microalga Chlorella vulgaris as a potential feedstock for biodiesel. Journal of Chemical Technology & Biotechnology 87: 137-145
Pubmed: Author and Title
CrossRef: Author and Title
Google Scholar: Author Only Title Only Author and Title

McCourt P, Desveaux D (2010) Plant chemical genetics. New Phytol 185: 15-26
Pubmed: Author and Title
CrossRef: Author and Title
Google Scholar: Author Only Title Only Author and Title

Morita E, Kumon Y Fau - Nakahara T, Nakahara T Fau - Kagiwada S, Kagiwada S Fau - Noguchi T, Noguchi T (2006) Docosahexaenoic acid production and lipid-body formation in Schizochytrium limacinum SR21. Marine Biotechnology 8: 319-327
Pubmed: Author and Title
CrossRef: Author and Title
Google Scholar: Author Only Title Only Author and Title

Msanne J, Xu D, Konda AR, Casas-Mollano JA, Awada T, Cahoon EB, Cerutti H (2012) Metabolic and gene expression changes triggered by nitrogen deprivation in the photoautotrophically grown microalgae Chlamydomonas reinhardtii and Coccomyxa sp C-

169. Phytochemistry 75: 50-59
Pubmed: Author and Title
CrossRef: Author and Title
Google Scholar: Author Only Title Only Author and Title

Rosenberg JN, Kobayashi N, Barnes A, Noel EA, Betenbaugh MJ, Oyler GA (2014) Comparative analyses of three Chlorella species in response to light and sugar reveal distinctive lipid accumulation patterns in the Microalga C. sorokiniana. PLoS One 9: e92460
Pubmed: Author and Title
CrossRef: Author and Title
Google Scholar: Author Only Title Only Author and Title

Sak K (2014) Cytotoxicity of dietary flavonoids on different human cancer types. Pharmacogn Rev 8: 122-146
Pubmed: Author and Title
CrossRef: Author and Title
Google Scholar: Author Only Title Only Author and Title

Schaffer JE (2003) Lipotoxicity: when tissues overeat. Current opinion in lipidology 14: 281
Pubmed: Author and Title
CrossRef: Author and Title
Google Scholar: Author Only Title Only Author and Title

Scranton MA, Ostrand JT, Fields FJ, Mayfield SP (2015) Chlamydomonas as a model for biofuels and bio-products production. Plant J 82: 523-531
Pubmed: Author and Title
CrossRef: Author and Title
Google Scholar: Author Only Title Only Author and Title

Song X, Zang X Fau - Zhang X, Zhang X (2015) Production of high docosahexaenoic acid by Schizochytrium sp. using low-cost raw materials from food industry J Oleo Sci 64: 197-204
Pubmed: Author and Title
CrossRef: Author and Title
Google Scholar: Author Only Title Only Author and Title

Specht EA, Nour-Eldin HH, Hoang KT, Mayfield SP (2015) An improved ARS2-derived nuclear reporter enhances the efficiency and ease of genetic engineering in Chlamydomonas. Biotechnol J 10: 473-479
Pubmed: Author and Title
CrossRef: Author and Title
Google Scholar: Author Only Title Only Author and Title

Sung B, Chung HY, Kim ND (2016) Role of Apigenin in Cancer Prevention via the Induction of Apoptosis and Autophagy. J Cancer Prev 21: 216-226
Pubmed: Author and Title
CrossRef: Author and Title
Google Scholar: Author Only Title Only Author and Title

Unger RH, Scherer PE (2010) Gluttony, sloth and the metabolic syndrome: a roadmap to lipotoxicity. Trends Endocrinol Metab 21: 345-352
Pubmed: Author and Title
CrossRef: Author and Title
Google Scholar: Author Only Title Only Author and Title

Urzica EI, Vieler A, Hong-Hermesdorf A, Page MD, Casero D, Gallaher SD, Kropat J, Pellegrini M, Benning C, Merchant SS (2013) Remodeling of Membrane Lipids in Iron-starved Chlamydomonas. Journal of Biological Chemistry 288: 30246-30258
Pubmed: Author and Title
CrossRef: Author and Title
Google Scholar: Author Only Title Only Author and Title

Wallace I, Bader G, Giaever G, Nislow C (2011) Displaying Chemical Information on a Biological Network Using Cytoscape. In G Cagney, A Emili, eds, Network Biology, Vol 781. Humana Press, pp 363-376
Pubmed: Author and Title
CrossRef: Author and Title
Google Scholar: Author Only Title Only Author and Title

Wan M-X, Wang R-M, Xia J-L, Rosenberg JN, Nie Z-Y, Kobayashi N, Oyler GA, Betenbaugh MJ (2012) Physiological evaluation of a new Chlorella sorokiniana isolate for its biomass production and lipid accumulation in photoautotrophic and heterotrophic cultures. Biotechnology and Bioengineering 109: 1958-1964
Pubmed: Author and Title
CrossRef: Author and Title
Google Scholar: Author Only Title Only Author and Title

Wang D, Lu Y, Huang H, Xu J (2012) Establishing oleaginous microalgae research models for consolidated bioprocessing of solar energy. Advances in biochemical engineering/biotechnology 128: 69-84
Pubmed: Author and Title
CrossRef: Author and Title
Google Scholar: Author Only Title Only Author and Title

Wase N, Black PN, Stanley BA, DiRusso CC (2014) Integrated quantitative analysis of nitrogen stress response in Chlamydomonas reinhardtii using metabolite and protein profiling. J Proteome Res 13: 1373-1396
Pubmed: Author and Title
CrossRef: Author and Title
Google Scholar: Author Only Title Only Author and Title

Wase N, Tu BQ, Black PN, DiRusso CC (2015) Phenotypic screening identifies Brefeldin A/Ascotoxin as an inducer of lipid storage in the algae Chlamydomonas reinhardtii. Algal Research-Biomass Biofuels and Bioproducts 11: 74-84
Pubmed: Author and Title
CrossRef: Author and Title
Google Scholar: Author Only Title Only Author and Title

Weng CJ, Yen GC (2012) Flavonoids, a ubiquitous dietary phenolic subclass, exert extensive in vitro anti-invasive and in vivo anti-metastatic activities. Cancer Metastasis Rev 31: 323-351
Pubmed: Author and Title
CrossRef: Author and Title
Google Scholar: Author Only Title Only Author and Title

Wetzel S, Klein K, Renner S, Rauh D, Oprea TI, Mutzel P, Waldmann H (2009) Interactive exploration of chemical space with Scaffold Hunter. Nat Chem Biol 5: 581-583
Pubmed: Author and Title
CrossRef: Author and Title
Google Scholar: Author Only Title Only Author and Title

Yeung N, Cline MS, Kuchinsky A, Smoot ME, Bader GD (2002) Exploring Biological Networks with Cytoscape Software. In Current Protocols in Bioinformatics. John Wiley & Sons, Inc.
Pubmed: Author and Title
CrossRef: Author and Title
Google Scholar: Author Only Title Only Author and Title

Zhang JH, Chung TD, Oldenburg KR (1999) A Simple Statistical Parameter for Use in Evaluation and Validation of High Throughput Screening Assays. J Biomol Screen 4: 67-73
Pubmed: Author and Title
CrossRef: Author and Title
Google Scholar: Author Only Title Only Author and Title